[AMERICAN JOURNAL OF SCIENCE, VOL. 306, NOVEMBER, 2006, P. 683–711, DOI 10.2475/09.2006.01]

American Journal of Science

NOVEMBER 2006

AGE AND DURATION OF ECLOGITE-FACIES METAMORPHISM, NORTH QAIDAM HP/UHP TERRANE, WESTERN CHINA

C. G. MATTINSON*, J. L. WOODEN**, J. G. LIOU*, D. K. BIRD*, and C. L. WU***

ABSTRACT. Amphibolite-facies para-and orthogneisses near Dulan, at the southeast end of the North Qaidam terrane, enclose minor eclogite and peridotite which record ultra-high pressure (UHP) metamorphism associated with the Early Paleozoic continental collision of the Qilian and Qaidam microplates. Field relations and coesite inclusions in zircons from paragneiss suggest that felsic, mafic, and ultramafic rocks all experienced UHP metamorphism and a common amphibolite-facies retrogression. SHRIMP-RG U-Pb and REE analyses of zircons from four eclogites yield weighted mean ages of 449 to 422 Ma, and REE patterns (flat HREE, no Eu anomaly) and inclusions of garnet, omphacite, and rutile indicate these ages record eclogite-facies metamorphism. The coherent field relations of these samples, and the similar range of individual ages in each sample suggests that the ~25 m.y. age range reflects the duration of eclogite-facies conditions in the studied samples. Analyses from zircon cores in one sample yield scattered 433 to 474 Ma ages, reflecting partial overlap on rims, and constrain the minimum age of eclogite protolith crystallization. Inclusions of Th + REE-rich epidote, and zircon REE patterns are consistent with prograde metamorphic growth. In the Lüliang Shan, approximately 350 km northwest in the North Qaidam terrane, ages interpreted to record eclogite-facies metamorphism of eclogite and garnet peridotite are as old as 495 Ma and as young as 414 Ma, which suggests that processes responsible for extended high-pressure residence are not restricted to the Dulan region. Evidence of prolonged eclogite-facies metamorphism in HP/UHP localities in the Northeast Greenland eclogite province, the Western Gneiss Region of Norway, and the western Alps suggests that long eclogite-facies residence may be globally significant in continental subduction/collision zones.

INTRODUCTION

Ultra-high pressure (UHP) metamorphism, defined by the pressure-temperature conditions of the coesite stability field (P > 27 kbar, depths > 80 km), is a product of continental subduction and collision. Since the discovery of metamorphic coesite (Chopin, 1984; Smith, 1984) and diamond (Sobolev and Shatsky, 1990), UHP terranes have been documented from more than 15 localities (for example, Liou and others, 2002). Typically, evidence of UHP metamorphism is preserved as rare mineral inclusions or relict mineral assemblages within host rocks that equilibrated at crustal conditions. Rapid exhumation from UHP conditions is commonly invoked (for example, Gebauer and others, 1997; Cong and others, 2000; Brueckner and van Roermund, 2004) to preserve the unusual UHP assemblages from thermal overprinting (Hacker and Peacock, 1995). Careful geochronological studies, linked to P-T conditions, have documented rapid (cm/a, similar to horizontal plate velocities) exhumation in several localities (for example, the Alps: Gebauer and others, 1997; Amato and others, 1999; Liati and Gebauer, 1999; Rubatto and Hermann, 2001;

*Department of Geological and Environmental Sciences, Stanford University, Stanford, California 94305-2115, U.S.A.; cgm@pangea.stanford.edu

**United States Geological Survey, 345 Middlefield Road, Menlo Park, California 94025, U.S.A.

***Chinese Academy of Geological Sciences, Institute of Geology, Beijing 100037, China

Rubatto and Scambelluri, 2003; Kokchetav: Hermann and others, 2001; Hacker and others, 2003b; Norway: Terry and others, 2000; Carswell and others, 2003; Hacker and others, 2003a; Betic Cordilleras: de Jong, 2003; Papua New Guinea: Baldwin and others, 2004, 2005; the Bohemian Massif and the Himalaya: Massonne and O'Brien, 2003).

Multiple metamorphic or igneous events, which may be individually of brief duration, are proposed to explain the significant range of ages observed in some localities (for example, Rubatto and Scambelluri, 2003; Brueckner and van Roermund, 2004; Hacker and Gans, 2005), but evidence for protracted (several to 10s of m.y.) residence at high-pressure conditions preserved in other areas (for example, Hacker, unpublished data; Hacker and others, 2000; Lapen and others, 2003; Kylander-Clark and others, 2005; McClelland and others, 2006) requires an alternative to the model of rapid subduction immediately followed by rapid exhumation, such as slow subduction or refrigeration by continued, structurally deeper subduction (for example, Hacker and others, 2000). Relatively few studies have constrained the rate and duration of subduction and prograde metamorphism, but both fast subduction rates (for example, Liati and Gebauer, 1999; Kaneko and others, 2003; Leech and others, 2005), similar to modern subduction rates of oceanic crust (England and others, 2004), and slow (<5 mm/a; Rubatto and others, 1999; Lapen and others, 2003) subduction rates have been reported.

The North Qaidam HP/UHP terrane is a major, Early Paleozoic continental suture zone in central Asia (fig. 1). Although existing geochronological constraints on the age of HP/UHP metamorphism are limited, eclogite and garnet peridotite record

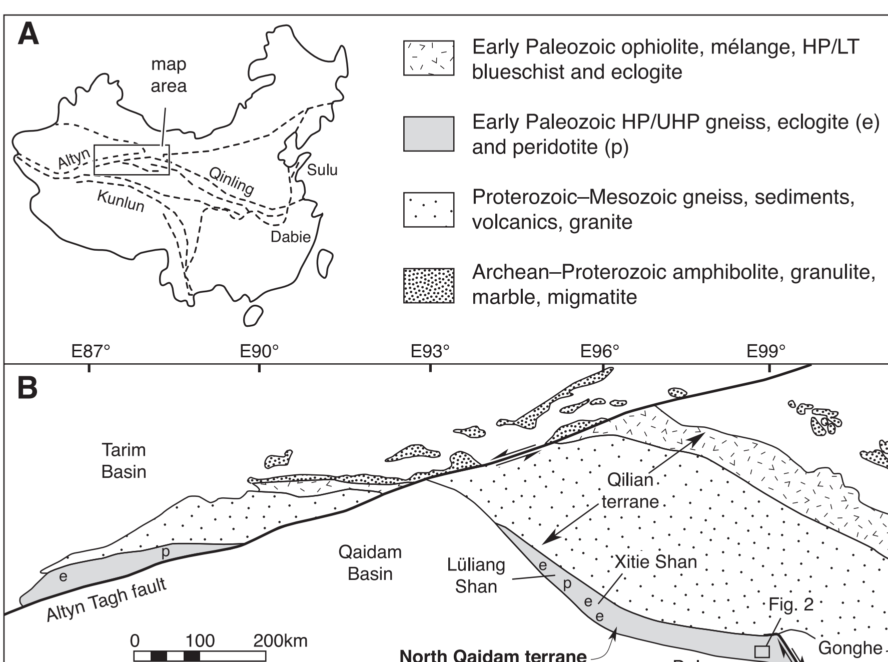

Fig. 1. (A) Map of China showing the location of this study (box) and the trends of major mountain belts (dashed lines). (B) Schematic map of the Qaidam-Qilian-Altyn Tagh region showing major tectonic units, and locations of eclogite and garnet peridotite. The box near Dulan (lower right corner) indicates the location of figure 2. Modified from Zhang and others (2005a).

a range of ages (423 – 497 Ma; Yang and others, 2001a, 2001b, 2002; Song and others, 2003a, 2005, 2006; Zhang and others, 2005b). Here we present SHRIMP-RG U-Pb geochronology and REE geochemistry of zircons from eclogite near Dulan (figs. 1 and 2), at the southeast end of the North Qaidam terrane, to examine the age and duration of their Early Paleozoic eclogite-facies metamorphism.

GEOLOGIC BACKGROUND

The northwest-southeast trending North Qaidam terrane records Early Paleozoic continental collision, and is bounded on the southwest by the Qaidam Basin, and on the northeast by the Qilian terrane (fig. 1; Yang and others, 2001b). The basement of the North Qaidam terrane is the Proterozoic Dakendaban Group gneiss, which is overlain by Paleozoic metasediments, and intruded by granites. The Dakendaban Group includes paragneiss, orthogneiss, marble, amphibolite, migmatite, and locally eclogite and garnet peridotite (Yang and others, 1994, 1998, 2001b, 2001c). The occurrence of marble and mature sediments such as biotite quartzite is consistent with deposition in a passive margin environment, and the presence of Paleoproterozoic to Late Archean zircons within paragneiss suggests that some sediments have a continental cratonal source. Eclogite occurs over a distance of 350 km in the Lüliang Shan, Xitie Shan, and near Dulan (figs. 1 and 2). The eclogite and peridotite occur as blocks, boudins or layers in the host para-and orthogneiss, and typically are 10s to <1 m across (fig. 3A). Zircon U-Pb ages from gneiss, eclogite, and peridotite of the North Qaidam

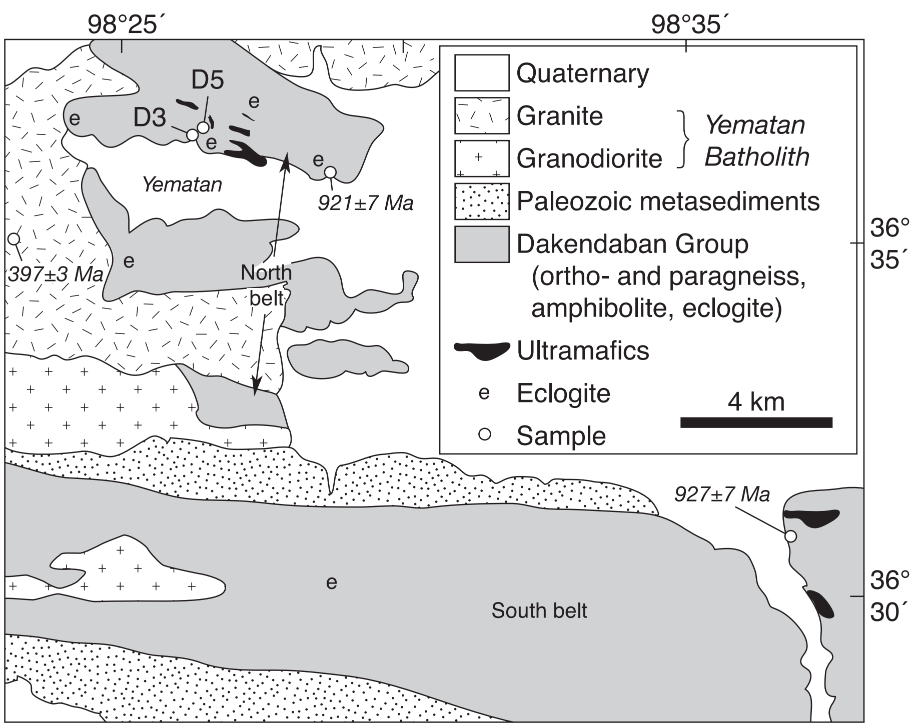

Fig. 2. Geologic sketch map of the study area showing sample locations. Foliation in the Dakendaban Group is dominantly northwest striking, steeply northeast dipping, locally modified by tight, northwest plunging folds. Granite and granodiorite are part of the Yematan batholith (397 ± 3 Ma; Wu and others, 2004). Magmatic ages of two Dakendaban Group granitic gneiss samples are from Mattinson and others (2006). The town of Dulan is approximately 30 km southwest of map area. Modified from Song and others (2003a) and Wu and others (2004).

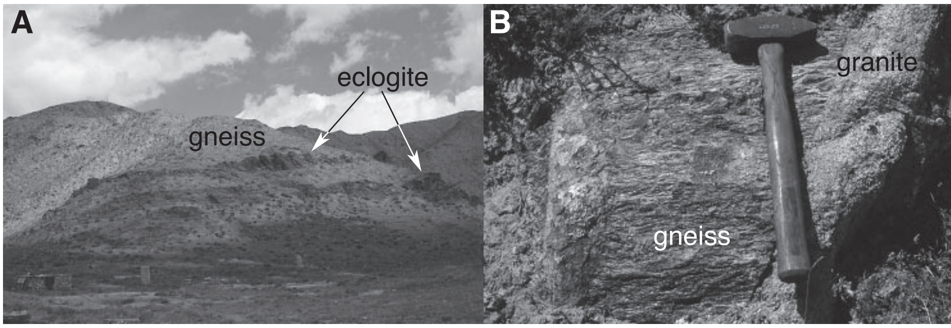

Fig. 3. (A) Eclogite layers in paragneiss, Dulan area, view to the northeast. The sample collection sites for this study are to the left of the area shown in the photograph. (B) Truncation of foliation in paragneiss by granite of the Yematan batholith.

terrane have been interpreted to record peak metamorphism between 423 to 497 Ma, similar to Sm-Nd garnet–omphacite–whole-rock isochron ages from eclogite (Yang and others, 2001a, 2001b, 2002; Song and others, 2003a, 2005, 2006; Zhang and others, 2005b).

The granites cross-cut the regional foliation, and crystallized between 397 to 456 Ma, which is thought to be coeval with continental collision between the North Qaidam and Qilian terranes (Wu and others, 2001, 2004; Gehrels and others, 2003a). North of the North Qaidam terrane, granites in the southern Qilian terrane (fig. 1) have I-type geochemistry, 425 to 496 Ma ages, and are interpreted to represent arc magmatism (Wu and others, 2001; Gehrels and others, 2003a). The subduction polarity responsible for convergence, magmatism, and subsequent collision of the North Qaidam and Qilian terranes is unclear, and models involving both north-dipping subduction (Yin and Harrison, 2000; Yang and others, 2001b, 2002; Song and others, 2006) and south-dipping subduction (Gehrels and others, 2003a, 2003b) have been proposed. Additional field and geochronological work is required to resolve this problem.

Near Dulan, collision-related granite and granodiorite of the Yematan batholith (fig. 2) cross-cut the northwest striking amphibolite-facies foliation in the Dakendaban Group gneisses (fig. 3B), and yield a U-Pb zircon age of 397 ± 3 Ma (Wu and others, 2001, 2004). Song and others (2003a, 2003b) distinguish northern and southern outcrop belts (fig. 2), and report peak P-T conditions for eclogites of 29 to 32 kbar, 631 to 687°C (north belt) and 29 to 33 kbar, 729 to 746°C (south belt). The discovery of coesite included in zircon from the host paragneiss confirms that both the mafic/ultramafic rocks and the felsic host gneiss were metamorphosed at UHP conditions (Song and others, 2001a, 2001b, 2003b, 2006; Yang and others, 2001c). Retrograde conditions are not quantitatively constrained for the north belt eclogites, but south belt eclogites record granulite-facies (19 – 20 kbar, 873 – 948°C) and amphibolite-facies (7 – 9 kbar, 660 – 695°C) retrogression (Song and others, 2003b). Two Sm-Nd garnet–omphacite–whole-rock isochrons of eclogite from the north belt yield ages of 458 ± 10 Ma and 459 ± 3 Ma (Song and others, 2003a), in agreement with a 457 ± 7 Ma zircon age from the same eclogite body (Song and others, 2006), but significantly older than a 423 ± 6 Ma zircon age from coesite-bearing paragneiss (Song and others, 2006). One Sm-Nd garnet–omphacite–whole-rock isochron of eclogite from the south belt yields an age of 497 ± 87 Ma (Song and others, 2003a). Granitic orthogneiss, commonly distinguished by cm-size augen, is interlayered with paragneiss at 10s to 100s of meter scale and both rock types share a common foliation. The original contact relationship (depositional, intrusive, tectonic) between ortho-and paragneiss is unclear, but inclusions of metasediments (Wan and others, 2006) and inherited zircons (Mattinson and others, 2006) in orthogneiss, and similar 1.9 to 2.2 Ga Nd depleted mantle model ages in both rock types (Wan and others, 2006) suggests an intrusive relationship and that the orthogneiss may have been derived from partial melting of the paragneiss. Our recent zircon U-Pb geochronology from Dakendaban Group granitic orthogneiss near Dulan (fig. 2) indicates magmatic crystallization at ca. 925 Ma, and ages from zircon rims (397 – 618 Ma) are compatible with minor recrystallization during *in situ* Ordovician-Silurian metamorphism (Mattinson and others, 2005, 2006). All rock types were subsequently uplifted and eroded during Cenozoic deformation associated with the India-Asia collision. Eclogite samples examined in this study were collected in the northern outcrop belt (fig. 2) near the coesite-bearing paragneiss and UHP eclogite described by Song and others (2003a, 2003b, 2006).

SAMPLE DESCRIPTION

Four eclogite samples from two localities were collected for zircon U-Pb geochronology (fig. 2). The eclogites occur as unfoliated or weakly foliated layers within strongly foliated garnet (± kyanite ± tourmaline) paragneiss. Eclogite D5A (collected at N36°36.39′, E98°26.33′) contains garnet (1 – 4 mm), omphacite, minor epidote, amphibole, rutile, and zircon. The omphacite is partially replaced by a symplectite of sodic augite and plagioclase, and pale green amphibole occurs along garnet grain boundaries. Veins of green amphibole, iron-rich epidote, and minor hematite, opaque minerals, and andradite cut across the eclogite-facies assemblage; plagioclase, calcite and minor chlorite in the vein centers appear to be the last-formed minerals. Zircon occurs as inclusions in garnet, omphacite, and epidote associated with the eclogite-facies assemblage. Several garnet cores contain blocky polycrystalline inclusions of clinozoisite ± amphibole (figs. 4A and 4B).

Eclogite D5B (collected at N36°36.39′, E98°26.33′) contains abundant garnet (5 – 10 mm, 70 – 80 vol%), omphacite, minor fine-grained intergrown muscovite and biotite, probably pseudomorphic after phengite, pale gray amphibole, epidote, apatite, rutile, and zircon. Minor symplectite replaces omphacite along grain boundaries, and amphibole occurs along garnet grain boundaries. The eclogite-facies assemblage is cut by veins similar to those in sample D5A. Zircon occurs as inclusions in eclogitic garnet.

Eclogite D3F (collected at N36°36.35′, E98°26.24′) contains garnet (2 – 3 mm), omphacite (mostly replaced by symplectite), quartz, epidote, rutile, and zircon. Zircon occurs as inclusions in garnet and epidote associated with the eclogite-facies assemblage. Garnet cores commonly contain inclusions of pale brown amphibole and blocky polycrystalline clinozoisite ± amphibole (fig. 4D).

Eclogite D3G (collected at N36°36.35′, E98°26.24′) is similar to D3F, but finer-grained, and contains garnet (0.5 – 1 mm), omphacite (mostly replaced by symplectite), quartz, epidote, rutile, and zircon. Garnet cores commonly contain inclusions of pale brown amphibole and blocky polycrystalline clinozoisite ± amphibole (fig. 4C).

ANALYTICAL METHODS

Zircon U-Pb geochronology and trace element analyses were performed in separate analytical sessions using the Stanford/USGS SHRIMP-RG (sensitive high-resolution ion micro-probe reverse geometry) facility. Zircon grains separated from the samples were mounted with zircon age standard R33 (Black and others, 2004) in a 2.54 cm epoxy disc and polished to approximate half-sections prior to reflected light and cathodoluminescence (CL) imaging. Cathodoluminescence images were collected using a JEOL 5600LV scanning electron microscope equipped with a Hamamatsu photomultiplier tube. Locations of SHRIMP analyses were chosen to avoid cracks, pits,

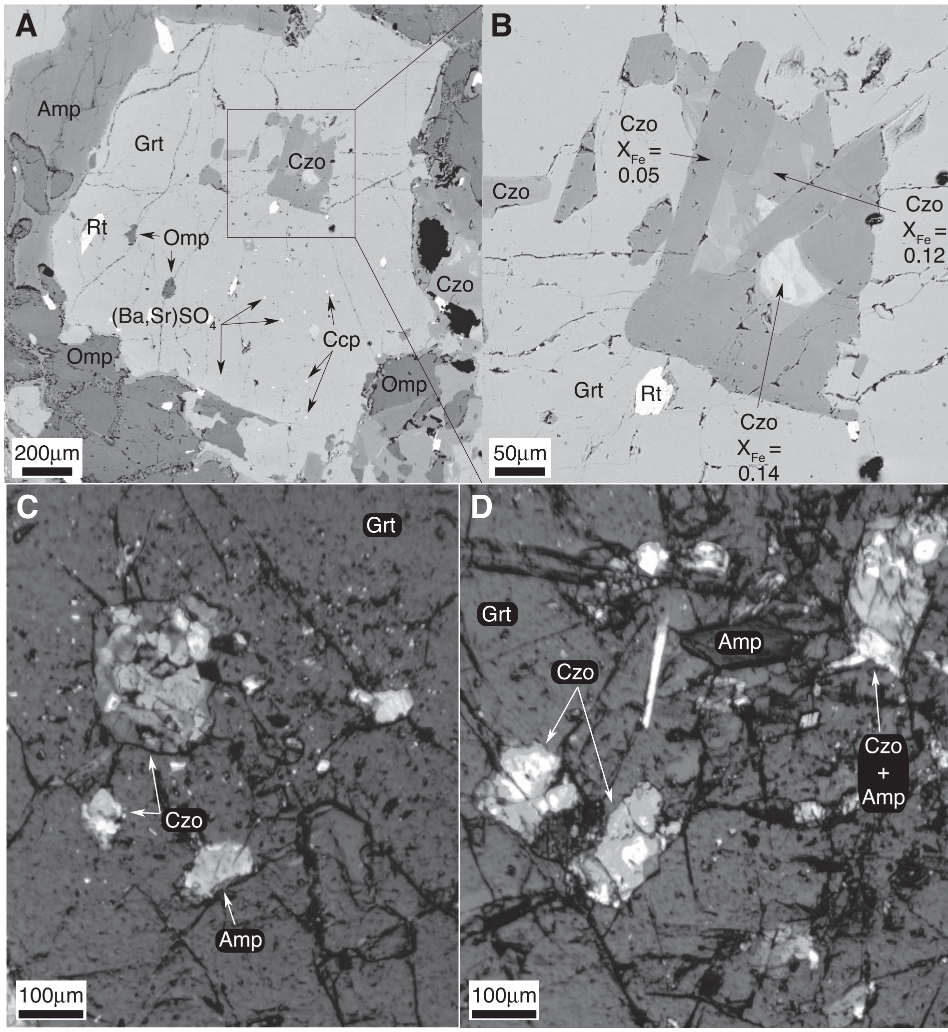

Fig. 4. Backscattered electron (BSE) images and photomicrographs of the studied samples. (A) BSE image (brightness proportional to average atomic number) of eclogite D5A showing blocky polycrystalline clinozoisite inclusions in the core, and omphacite, (Ba, Sr)SO_4, and (Cu, Fe, S; chalcopyrite?) inclusions in the garnet rim. (B) Enlarged view of A showing different clinozoisite compositions within a single inclusion. The bright area (labeled X_{Fe} = 0.14) contains REE (EDS analysis) and low Ca (fig. 9A), consistent with REE ± Sr incorporation. (C) Photomicrograph of amphibole and polycrystalline clinozoisite in garnet, eclogite D3G. Partially crossed polars. (D) Photomicrograph of amphibole, polycrystalline clinozoisite, and polycrystalline clinozoisite + amphibole in garnet, eclogite D3F. Partially crossed polars. Mineral abbreviations follow Kretz (1983).

or inclusions identified in CL and reflected light images. The sample was coated with high-purity Au, and placed under high vacuum for one day prior to analysis to minimize interference from gas species.

The analytical routine for U-Pb geochronology followed Williams (1998), and age calculations were performed using the Isoplot and Squid programs (Ludwig, 2001, 2003) and IUGS recommended decay constants (Steiger and Jäger, 1977). The sample was sputtered by a ~5 nA O_2^- primary beam focused to ~30 µm diameter, and the mass resolution was 6000 to 7000 at 10 percent peak height. Prior to analysis, the primary ion beam was rastered across the grain surface to remove the Au-coating and any surface contamination. Each analysis comprised 6 scans of peaks corresponding to $^{90}Zr_2{}^{16}O$, ^{204}Pb, background, ^{206}Pb, ^{207}Pb, ^{208}Pb, ^{238}U, $^{232}Th^{16}O$ and $^{238}U^{16}O$, with count times of 2 to 20 s for each peak. The concentration of U was calibrated using zircon standard CZ3 (U = 550 ppm; Pidgeon and others, 1994), and the Pb/U ratio was calibrated using zircon age standard R33 (419 Ma; Black and others, 2004). The calibration error for the $^{206}Pb/^{238}U$ ratios of R33 is 0.50 percent (2σ; table 1), and is included in the uncertainty for weighted mean ages, but not for individual analyses, as all analyses are from a single analytical session. Estimates of common Pb compositions use the two-stage Pb evolution model of Stacey and Kramers (1975). Individual ages reported below are $^{206}Pb/^{238}U$ ages corrected for common Pb using ^{207}Pb (Williams, 1998) unless otherwise noted, and errors for weighted mean ages from multiple analyses are given at 95 percent confidence.

For trace element analyses, we selected one isotope to represent each element, based on abundance and absence of significant interferences, similar to the approach of Maas and others (1992). Each analysis comprised 3 scans of peaks corresponding to ^{30}Si, ^{31}P, $^{28}Si^{16}O_2$, ^{89}Y, ^{96}Zr, ^{139}La, ^{140}Ce, ^{146}Nd, ^{147}Sm, ^{153}Eu, $^{141}Pr^{16}O$, ^{157}Gd, ^{163}Dy, $^{166}Er^{16}O$, $^{172}Yb^{16}O$, $^{175}Lu^{16}O$, $^{180}Hf^{16}O$, ^{232}Th, and ^{238}U, with count times of 2 to 8 s for each peak. Operating at ~8500 mass resolution at 10 percent peak height, these peaks are well resolved from LREE oxides and Zr, Si, O molecules. Primary beam current and spot size were similar to those used for geochronology. Sri Lankan gem zircon SL13 was analyzed as a concentration standard (fig. 5A; table 2), and after every 12 unknowns, Sri Lankan gem zircon CZ3 was analyzed to monitor instrument stability (fig. 5B; table 2). The raw data were converted to ppm by normalizing average count rates to ^{30}Si, correcting for natural isotopic abundance, and calibrating concentrations to trace element values for zircon standard SL13 reported by Hoskin (1998), except for P, which was calibrated to NIST SRM 611 and 613 glass values reported by Pearce and others (1997). Conversion of these concentrations to chondrite-normalized patterns (Coryell and others, 1963) uses the recommended CI carbonaceous chondrite composition of McDonough and Sun (1995). The 40 analyses of CZ3 (fig. 5B; table 2) provide a conservative estimate of the uncertainty of the trace element analyses. Standard deviations of the REE are 10 to 15 percent, except for La (32%) and Pr (22%) due to low abundance. Standard deviations of P, Y, Hf, Th, and U are 5 to 10 percent. The consistency of the REE patterns suggests that part of this variability reflects true sample variation. The agreement between U concentrations measured during U-Pb analysis and trace element analysis (fig. 6) indicates that the trace element measurements may be applied to the interpretation of the U-Pb measurements for most analyses.

Mineral chemistry was determined with an automated JEOL 733A electron microprobe at Stanford University with operating conditions of 15 nA beam current, and 15 keV accelerating potential, calibrated on natural mineral standards. Raw counts were collected for 20 s and converted to oxide weight percent by the CITZAF correction procedure. Minerals were analyzed with a focused (<2 μm) beam. Energy dispersive (EDS) analysis was used to assess the presence of Zr, REE, Th, Ba, Sr, and S, which were not analyzed quantitatively. Analyses of inclusions in zircon that contained detectable Zr are excluded from the figures and tables. The slightly low totals for some analyses (table 3) probably reflects interference from the adjacent zircon that was below the detection limit of EDS.

RESULTS

Eclogite D5A

Most zircons from eclogite D5A contain two or more concentric zones defined by differences in CL brightness (figs. 7A and 7C). The innermost zone is typically a CL

TABLE 1

Zircon U-P isotopic data, North Qaidam eclogite samples D5A, D5B, D3F, and D3G

Analysis	CL	$^{206}Pb_c$ (%)	U (ppm)	Th (ppm)	$^{232}Th/^{238}U$	$^{206}Pb^*$ (ppm)	$^{206}Pb/^{238}U$ Age* (Ma, ±1σ)	Total $^{238}U/^{206}Pb$ (± % err)	Total $^{207}Pb/^{206}Pb$ (± % err)
D5A-1†	m	0.00	253	16	0.07	15.8	451.7 ± 1.9	13.8 ± 0.4	0.0560 ± 1.4
D5A-2†	m	0.38	109	9	0.09	6.7	445.1 ± 2.8	13.9 ± 0.6	0.0589 ± 2.1
D5A-3	d	--	648	90	0.14	39.5	441.8 ± 1.1	14.1 ± 0.3	0.0550 ± 0.9
D5A-4†	b	0.18	12	0.2	0.02	0.8	457.9 ± 9.3	13.6 ± 2.0	0.0576 ± 7.3
D5A-5	d	--	274	12	0.04	16.4	436.3 ± 1.7	14.3 ± 0.4	0.0553 ± 1.4
D5A-6	c	0.07	146	37	0.26	9.4	464.7 ± 2.4	13.4 ± 0.5	0.0569 ± 1.8
D5A-7†	m	0.19	53	7	0.14	3.3	444.0 ± 3.9	14.0 ± 0.9	0.0573 ± 3.1
D5A-8†	m	0.13	59	2	0.04	3.7	452.6 ± 3.7	13.7 ± 0.8	0.0570 ± 2.9
D5A-9†	m	0.19	62	2	0.04	3.7	440.0 ± 3.6	14.1 ± 0.8	0.0572 ± 2.8
D5A-10†	b	--	18	0.4	0.02	1.1	454.9 ± 6.9	13.7 ± 1.5	0.0545 ± 5.5
D5A-11†	m	--	140	10	0.08	8.7	451.8 ± 2.4	13.8 ± 0.5	0.0557 ± 1.9
D5A-12	d	0.04	212	25	0.12	12.3	421.2 ± 1.9	14.8 ± 0.4	0.0556 ± 2.0
D5A-13†	m	--	132	11	0.09	8.2	450.8 ± 2.6	13.8 ± 0.6	0.0551 ± 2.0
D5A-14†	m	--	97	4	0.04	6.0	446.7 ± 3.0	14.0 ± 0.7	0.0546 ± 2.4
D5A-15†	m	0.04	184	2	0.01	11.3	445.2 ± 2.1	14.0 ± 0.5	0.0561 ± 1.7
D5A-16	c	0.18	303	209	0.71	19.8	471.0 ± 1.7	13.2 ± 0.4	0.0580 ± 1.3
D5A-17	m	0.16	71	10	0.14	4.1	416.0 ± 3.2	15.0 ± 0.8	0.0564 ± 2.8
D5A-18†	b	0.17	38	3	0.07	2.4	457.0 ± 4.7	13.6 ± 1.0	0.0575 ± 3.6
D5A-19†	m	0.33	100	10	0.10	6.1	442.0 ± 2.8	14.0 ± 0.6	0.0584 ± 2.2
D5A-20	b	0.51	26	0.8	0.03	1.5	419.5 ± 5.5	14.8 ± 1.3	0.0593 ± 4.8
D5A-21	c	0.10	674	97	0.15	40.3	433.2 ± 1.1	14.4 ± 0.2	0.0564 ± 0.9
D5A-22	c	1.30	9	0.4	0.05	0.5	452.1 ± 10.2	13.6 ± 2.2	0.0666 ± 7.3
D5A-23	c	0.09	545	189	0.36	34.6	459.5 ± 1.3	13.5 ± 0.3	0.0569 ± 0.9
D5A-24	d	0.13	457	72	0.16	28.3	448.4 ± 1.4	13.9 ± 0.3	0.0570 ± 1.1
D5A-25	m	0.04	53	3	0.06	3.4	462.4 ± 4.0	13.4 ± 0.9	0.0566 ± 3.1
D5A-26†	m	0.08	272	3	0.01	16.9	450.9 ± 2.0	13.8 ± 0.4	0.0566 ± 1.4
D5A-27	d	0.18	186	42	0.23	10.5	410.3 ± 2.0	15.2 ± 0.5	0.0564 ± 1.7
D5A-28†	m	--	97	6	0.06	6.0	453.3 ± 3.0	13.8 ± 0.7	0.0537 ± 2.4
D5A-29	c	0.03	425	165	0.40	27.9	474.2 ± 1.5	13.1 ± 0.3	0.0568 ± 1.1
D5A-30	c	0.08	387	101	0.27	23.9	447.6 ± 1.5	13.9 ± 0.3	0.0565 ± 1.3
D5A-31	c	0.47	195	58	0.31	12.4	457.8 ± 2.1	13.5 ± 0.5	0.0600 ± 1.6
D5A-32	c	0.14	249	77	0.32	15.3	443.7 ± 2.0	14.0 ± 0.4	0.0569 ± 1.5
D5A-33	b	0.28	22	1.2	0.06	1.4	451.7 ± 6.8	13.7 ± 1.5	0.0583 ± 5.3
D5A-34	m	--	179	14	0.08	10.7	432.7 ± 3.2	14.4 ± 0.8	0.0553 ± 1.7
D5A-35†	b	--	17	0.2	0.01	1.0	447.8 ± 7.1	13.9 ± 1.6	0.0554 ± 6.2
D5A-36†	m	0.42	23	0.2	0.01	1.4	451.5 ± 5.9	13.7 ± 1.3	0.0593 ± 4.6
D5B-1	m	0.28	179	18	0.11	10.3	418.7 ± 2.0	14.9 ± 0.5	0.0574 ± 1.7
D5B-2†	b	0.00	34	0.9	0.03	2.0	432.0 ± 4.8	14.4 ± 1.1	0.0555 ± 4.0
D5B-3†	m	--	162	22	0.14	9.9	443.5 ± 2.2	14.0 ± 0.5	0.0556 ± 1.8
D5B-4†	m	--	160	12	0.08	9.8	443.2 ± 2.3	14.1 ± 0.5	0.0554 ± 1.8
D5B-5†	m	0.00	146	17	0.12	8.8	436.0 ± 2.4	14.3 ± 0.5	0.0556 ± 2.0
D5B-6†	d	0.22	238	59	0.25	14.1	427.8 ± 1.8	14.5 ± 0.4	0.0571 ± 1.5
D5B-7	b	0.24	37	2	0.06	2.3	444.8 ± 4.8	14.0 ± 1.1	0.0577 ± 3.8
D5B-8	d	0.10	243	15	0.06	14.1	420.6 ± 1.8	14.8 ± 0.4	0.0560 ± 1.5
D5B-9	m	0.18	202	24	0.12	12.8	459.1 ± 3.9	13.5 ± 0.9	0.0576 ± 1.6
D5B-10	b	--	46	5	0.10	2.9	453.5 ± 4.8	13.7 ± 1.1	0.0549 ± 3.4
D5B-11	b	0.02	59	4	0.08	3.6	435.4 ± 3.8	14.3 ± 0.9	0.0558 ± 3.1
D5B-12†	b	0.01	50	3	0.06	3.0	435.8 ± 4.0	14.3 ± 0.9	0.0557 ± 3.3

Table 1

(Continued)

Analysis	CL	$^{206}Pb_c$ (%)	U (ppm)	Th (ppm)	$^{232}Th/^{238}U$	$^{206}Pb^*$ (ppm)	$^{206}Pb/^{238}U$ Age* (Ma, ±1σ)	Total $^{238}U/^{206}Pb$ (± % err)	Total $^{207}Pb/^{206}Pb$ (± % err)
D5B-13†	d	0.05	201	46	0.24	12.2	440.5 ± 2.0	14.1 ± 0.5	0.0561 ± 1.6
D5B-14†	m	0.18	140	8	0.06	8.5	439.6 ± 2.5	14.1 ± 0.6	0.0572 ± 2.0
D5B-15†	m	0.23	52	2	0.05	3.1	431.0 ± 4.1	14.4 ± 0.9	0.0573 ± 3.3
D5B-16	b	0.12	75	6	0.08	4.4	424.0 ± 3.3	14.7 ± 0.8	0.0562 ± 2.8
D5B-17†	m	0.08	151	20	0.14	9.0	434.9 ± 3.1	14.3 ± 0.7	0.0562 ± 1.9
D5B-18	m	0.01	191	3	0.02	11.9	453.4 ± 2.2	13.7 ± 0.5	0.0561 ± 1.7
D5B-19†	m	--	240	23	0.10	14.7	444.4 ± 2.1	14.0 ± 0.5	0.0548 ± 1.5
D5B-20†	b	1.49	35	2	0.06	2.1	429.4 ± 5.5	14.3 ± 1.2	0.0675 ± 4.4
D3F-1†	m	0.37	9	0.4	0.04	0.5	417.5 ± 14.1	14.9 ± 3.4	0.0581 ± 9.7
D3F-2†	m	0.70	19	0.7	0.04	1.1	419.6 ± 8.8	14.8 ± 2.1	0.0608 ± 5.6
D3F-3	m	1.03	8	0.4	0.04	0.5	434.5 ± 13.3	14.2 ± 3.0	0.0639 ± 8.5
D3F-4†	m	0.12	24	0.6	0.02	1.4	416.8 ± 7.7	15.0 ± 1.8	0.0561 ± 5.5
D3F-5	m	0.83	19	3	0.15	1.2	437.6 ± 7.3	14.1 ± 1.7	0.0624 ± 4.7
D3F-6†	m	0.56	8	0.1	0.02	0.5	417.1 ± 10.9	14.9 ± 2.6	0.0597 ± 7.6
D3F-7†	m	0.37	30	1.4	0.05	1.7	424.4 ± 5.2	14.6 ± 1.2	0.0583 ± 4.4
D3F-8†	m	--	22	0.4	0.02	1.3	430.7 ± 6.1	14.5 ± 1.4	0.0538 ± 6.3
D3F-9†	m	--	15	1.3	0.09	0.9	426.0 ± 7.2	14.7 ± 1.7	0.0532 ± 6.2
D3F-10†	m	0.78	28	0.9	0.03	1.6	415.0 ± 5.3	14.9 ± 1.2	0.0614 ± 5.6
D3F-11†	m	0.96	15	0.2	0.01	0.9	431.7 ± 7.6	14.3 ± 1.7	0.0632 ± 7.8
D3F-12†	m	0.30	20	0.4	0.02	1.2	417.0 ± 6.1	14.9 ± 1.4	0.0575 ± 5.1
D3G-1	m	2.37	4	0	0.03	0.2	394.6 ± 15.4	15.5 ± 3.8	0.0737 ± 13.2
D3G-2	m	3.27	3	0	0.04	0.2	438.9 ± 18.6	13.7 ± 4.1	0.0821 ± 13.1
D3G-3	m	5.70	1	0	0.02	0.05	416.3 ± 31.3	14.1 ± 7.2	0.1012 ± 19.5
D3G-4	m	--	6	0	0.05	0.3	418.4 ± 11.9	15.0 ± 2.8	0.0484 ± 11.6
D3G-5	m	8.30	1	0	0.01	0.05	450.3 ± 37.1	12.7 ± 7.8	0.1232 ± 18.4
D3G-6	m	24.9	13	1	0.05	1.0	415.9 ± 32.8	11.3 ± 1.6	0.2562 ± 16.0
D3G-7	m	1.37	1	0	0.01	0.04	355.8 ± 29.3	17.4 ± 7.8	0.0647 ± 37.3
D3G-8	m	2.13	8	0	0.05	0.5	412.7 ± 9.8	14.8 ± 2.3	0.0722 ± 7.4

Note: Abbreviations: b, bright CL; c, dark CL core; d, dark CL whole grain; m, medium CL; Pb_c and Pb* denote the common and radiogenic portions, respectively. Samples were analyzed 30 June–1 July 2004, for which the error in standard calibration was 0.50% (2σ). The error in standard calibration is not included in the errors listed above, but is required when comparing data from different sessions, or with other geochronological data.

*Common Pb corrected by assuming $^{206}Pb/^{238}U$–$^{207}Pb/^{235}U$ age-concordance (^{207}Pb correction, Williams, 1998).

†Analysis included in weighted mean age calculation.

dark, inclusion-rich core, surrounded by one or more medium to bright CL, inclusion-poor zones, hereafter referred to as rims. A few grains are CL dark throughout (fig. 7E), but unlike the cores lack inclusions, and appear to comprise grain aggregates.

Eight analyses of the CL dark cores and one analysis of a bright CL core yield 9 to 674 ppm U (most analyses ~300 ppm), Th/U = 0.05 – 0.71, and 433 to 474 Ma ages which do not form a coherent group (figs. 7A, 7B and 8B; table 1). The REE patterns (fig. 7A) are characterized by steep HREE slopes (Lu_n/Gd_n = 40 – 154; most analyses ~90) and negative Eu anomalies ($Eu/Eu^* = Eu_n/(Sm_n \times Gd_n)^{0.5} = 0.26 – 0.62$; figs. 7A and 8A; table 2). Three analyses with Eu/Eu* = 0.89 – 0.99 have anomalously elevated LREE, and probably reflect overlap on LREE-rich inclusions (for example, fig. 7A, analysis 29). Inclusions in the zircon cores include epidote, rutile, and garnet. One

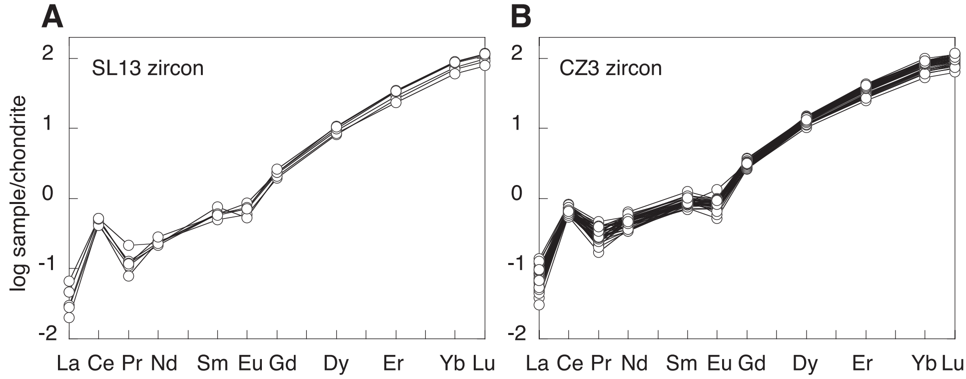

Fig. 5. Chondrite-normalized REE patterns (Coryell and others, 1963) for Sri Lankan gem zircons SL13 (A) and CZ3 (B). Normalized to chondrite values of McDonough and Sun (1995).

albite inclusion occurs within a crack and may be secondary, and a large epidote inclusion which nearly reaches the edge of the same zircon has a composition (two analyses in the upper right part of fig. 9A; table 3) similar to vein epidote, and probably reflects secondary growth or alteration. Two other zircons contain epidote inclusions with similar compositions to epidote/clinozoisite in the matrix as well as inclusions in garnet cores (fig. 9A; table 3). One garnet inclusion has a composition similar to garnet porphyroblasts, but is slightly higher in iron.

Nineteen analyses of the medium to bright CL rims yield 12 to 272 ppm U, Th/U = 0.01 – 0.14, and a weighted mean age of 448.9 ± 2.2 Ma (from 17 analyses, MSWD = 2.0, probability = 0.008; figs. 7C, 7D, and 8B; table 1). The REE patterns (fig. 7C) are characterized by flat HREE slopes (Lu_n/Gd_n = 2–55; most analyses ~10) and lack Eu anomalies (Eu/Eu* = 0.84 – 1.15; figs. 7C and 8A; table 2). Concentrations of Hf are similar in cores and rims, but rims contain lower P and Y (table 2). Sparse inclusions include garnet and omphacite. Analysis of one garnet inclusion yields a composition similar to that of garnet porphyroblasts (fig. 9B; table 3). None of the omphacite grains were large enough to analyze without overlap on the surrounding zircon.

Five analyses of the CL dark grains yield 186 to 648 ppm U, Th/U = 0.04 – 0.23, and 410 to 448 Ma ages which do not form a coherent group (figs. 7E, 7F, and 8B; table 1). The REE patterns are characterized by relatively steep HREE slopes (Lu_n/Gd_n = 39 – 86, except for one analysis), but differ from cores in their lack of Eu anomalies (Eu/Eu* = 0.98 – 1.21; figs. 7E and 8A; table 2). Concentrations of Hf overlap the lower range of core and rim values, and P and Y are intermediate relative to cores and rims (table 2). A few inclusions were visible beneath the grain surface, but none were exposed for analysis.

Two analyses (#20 and #33) that partially overlie cracks, yielded anomalous, irregular REE patterns (table 2; not plotted in fig. 7). These analyses are interpreted to reflect modification by post crystallization alteration, and are excluded from further discussion, as is an additional analysis (#25) that has a large mismatch (~2×) between U concentrations measured during U-Pb and REE analyses (tables 1 and 2), suggesting that the analyses did not sample the same zone.

Garnet-rich Eclogite D5B

Zircons from eclogite D5B include bright, medium, and dark CL zones (figs. 10A and 10C), but contain few of the inclusion-rich dark CL cores found in eclogite D5A.

TABLE 2

Zircon trace element data, North Qaidam eclogite samples D5A, D5B and D3F (abundance expressed in ppm)

sample	CL	La	Ce	Pr	Nd	Sm	Eu	Gd	Dy	Er	Yb	Lu	P	Y	Hf	Th	U	Ce/ Ce*	Eu/ Eu*	Lu_n/Gd_n
D5A-1	m	0.007	3.2	0.07	0.30	0.25	0.20	1.5	8.4	19	47	10	126	124	8253	12	230	36	0.97	55
D5A-2	m	0.006	2.4	0.08	0.49	0.52	0.44	2.9	6.4	4.3	4.4	0.80	65	47	9037	4	125	28	1.11	2
D5A-3	d	0.014	6.0	0.19	1.5	1.2	0.91	4.6	21	64	197	49	308	385	6796	81	723	28	1.18	86
D5A-4	b	0.06	0.46	0.02	0.11	0.10	0.07	0.51	2.3	3.8	7.7	1.6	58	28	9071	--	13	3	0.91	26
D5A-5	d	0.003	4.0	0.08	0.47	0.52	0.44	3.6	17	18	19	2.9	109	169	8712	--	320	68	0.98	6
D5A-6	c	0.08	2.2	0.12	0.36	0.40	0.14	2.6	18	53	159	37	270	310	11695	--	165	6	0.40	115
D5A-7	m	0.003	4.8	0.13	0.97	0.92	0.80	5.8	24	32	49	9.2	135	259	7847	--	68	56	1.05	13
D5A-8	m	0.008	2.1	0.05	0.36	0.47	0.35	2.8	9.6	9.1	12	2.0	86	85	7790	--	65	25	0.93	6
D5A-9	m	0.013	2.2	0.06	0.38	0.41	0.34	2.7	9.6	10	14	2.5	84	88	8624	--	70	19	1.00	8
D5A-10	b	0.10	1.1	0.10	0.39	0.26	0.18	1.4	5.6	7.6	14	2.9	48	63	8642	--	21	3	0.93	17
D5A-11	m	0.004	4.3	0.14	1.3	1.0	0.81	5.8	19	19	22	3.5	118	185	7209	--	153	41	1.01	5
D5A-12	d	0.02	3.9	0.12	0.84	0.89	0.65	3.6	13	28	74	17	143	184	7189	--	249	21	1.09	39
D5A-13	m	0.009	2.0	0.03	0.20	0.25	0.18	1.4	6.7	10	15	2.7	88	87	8078	--	126	28	0.90	15
D5A-14	m	0.54	2.3	0.05	0.46	0.57	0.60	4.6	11	8.4	9.4	1.5	76	86	8848	--	73	3	1.14	3
D5A-15	m	0.005	1.6	0.05	0.58	0.94	0.75	6.6	22	17	16	2.5	95	167	9336	--	221	24	0.91	3
D5A-16	c	0.05	8.9	0.16	1.2	1.7	0.42	15	99	225	527	113	826	1390	9998	--	363	24	0.26	60
D5A-17	m	0.02	1.0	0.06	0.36	0.39	0.32	1.9	4.7	6.6	11	2.3	61	51	11541	--	77	8	1.15	10
D5A-18	b	0.005	1.0	0.02	0.11	0.13	0.09	0.67	4.5	7.8	10	1.8	71	67	12077	--	49	25	0.95	22
D5A-19	m	0.006	3.0	0.08	0.45	0.52	0.40	2.9	12	14	19	3.2	84	131	9124	--	113	32	1.01	9
D5A-20	b	0.19	4.5	0.15	1.0	0.38	0.22	1.1	2.6	2.3	3.0	0.68	29	22	12291	--	46	6	1.03	5
D5A-21	c	0.015	30	0.68	3.5	2.4	1.8	12	53	116	305	67	423	816	6255	--	747	72	0.99	45
D5A-22	c	0.007	0.21	0.004	0.08	0.10	0.03	0.63	8.1	21	42	7.9	79	151	11221	--	7	9	0.37	102
D5A-23	c	1.6	26	5.1	14	3.0	1.5	7.3	32	73	197	44	254	478	10197	--	406	2	0.95	49
D5A-24	d	0.009	16	0.32	1.3	0.95	0.74	5.1	23	47	118	27	294	334	6521	--	503	74	1.02	42
D5A-25	m	0.005	3.7	0.07	0.40	0.28	0.24	1.7	8.2	16	39	8.4	108	120	6826	--	94	49	1.05	40
D5A-26	m	0.41	2.5	0.06	0.37	0.39	0.27	2.5	9.6	12	19	3.4	98	102	9470	--	207	4	0.84	11

TABLE 2
(Continued)

sample	CL	La	Ce	Pr	Nd	Sm	Eu	Gd	Dy	Er	Yb	Lu	P	Y	Hf	Th	U	Ce/ Ce*	Eu/ Eu*	Lu_n/ Gd_n
D5A-27	d	0.010	1.6	0.06	0.45	0.54	0.48	2.7	9.1	23	70	18	134	128	9743	--	308	16	1.21	54
D5A-28	m	0.011	3.2	0.08	0.61	0.66	0.51	3.9	14	14	15	2.3	88	140	7554	--	105	25	0.97	5
D5A-29	c	6.8	50	8.0	35	5.1	2.0	9.5	50	156	467	112	870	950	8860	--	517	2	0.89	95
D5A-30	c	5.5	19	2.1	11	1.6	0.42	7.5	58	197	618	143	745	1020	9226	--	471	1	0.37	154
D5A-31	c	0.13	4.0	0.18	1.6	1.8	0.48	13	73	145	310	64	1270	937	8990	59	214	6	0.30	40
D5A-32	c	0.06	3.1	0.09	0.63	0.58	0.29	3.6	21	55	157	37	286	346	11237	92	353	11	0.62	83
D5A-33	b	2.6	4.1	0.14	1.2	0.31	0.22	1.2	2.3	1.3	1.5	1.1	32	16	10122	1	25	2	1.12	7
D5A-34	m	0.008	2.6	0.05	0.29	0.28	0.20	1.6	8.9	18	42	9.3	116	125	7742	14	232	32	0.92	46
D5A-35	b	0.004	0.23	0.003	0.06	0.09	0.06	0.49	2.3	3.3	5.7	1.0	74	32	7722	0	16	16	0.86	17
D5A-36	m	0.14	0.77	0.03	0.23	0.17	0.11	0.80	4.0	5.8	9.7	2.0	76	49	9847	0	35	3	0.94	20
D5B-1	m	0.02	4.5	0.10	0.49	0.41	0.35	2.5	11	20	44	10	155	153	6250	18	211	27	1.06	32
D5B-2	b	0.007	0.61	0.02	0.16	0.18	0.12	0.71	1.1	0.74	0.99	0.22	27	9	13290	1	39	14	0.99	3
D5B-3	m	0.09	6.7	0.31	2.3	1.1	0.79	5.1	22	37	87	19	194	317	5517	17	180	10	1.01	30
D5B-4	m	0.008	4.5	0.08	0.44	0.37	0.31	2.0	9.9	19	46	11	114	142	6698	12	187	42	1.07	43
D5B-5	m	0.010	5.5	0.13	0.72	0.64	0.49	3.4	15	28	65	15	176	208	6424	16	170	37	1.01	34
D5B-6	d	0.03	4.9	0.19	1.8	1.5	0.99	4.1	4.2	3.1	3.9	0.69	60	35	7766	53	253	16	1.23	1
D5B-7	b	0.005	0.83	0.02	0.11	0.22	0.15	0.96	1.5	0.88	0.81	0.18	32	11	11661	2	38	22	1.01	2
D5B-8	d	0.03	2.8	0.12	1.1	0.85	0.65	3.1	7.0	5.9	6.9	1.2	84	66	7317	13	260	12	1.22	3
D5B-9	m	0.009	5.8	0.13	0.98	0.69	0.55	3.7	16	23	45	9.4	154	211	6797	23	232	41	1.05	20
D5B-10	b	0.55	1.9	0.22	1.2	0.50	0.37	2.0	2.6	1.2	1.2	0.21	49	18	8634	4	52	1	1.14	1
D5B-11	b	2.05	6.8	0.16	1.5	0.27	0.24	1.5	2.2	1.1	1.6	1.0	41	18	13317	5	72	3	1.17	6
D5B-12	b	0.007	0.80	0.02	0.13	0.17	0.11	0.73	1.3	0.82	0.96	0.20	36	11	10963	4	63	19	0.93	2
D5B-13	d	0.02	5.4	0.12	1.0	0.93	0.64	3.0	8.6	16	41	9.5	132	120	7691	29	180	27	1.15	25
D5B-14	m	0.005	2.4	0.05	0.35	0.32	0.26	1.6	3.0	2.0	2.6	0.53	70	23	7998	7	136	37	1.12	3

TABLE 2
(Continued)

sample	CL	La	Ce	Pr	Nd	Sm	Eu	Gd	Dy	Er	Yb	Lu	P	Y	Hf	Th	U	Ce/ Ce*	Eu/ Eu*	Lu_n/ Gd_n
D5B-15	m	0.009	1.8	0.06	0.63	0.86	0.73	4.3	5.6	2.6	2.7	0.43	42	37	8603	5	86	19	1.17	1
D5B-16	b	0.010	0.43	0.012	0.15	0.12	0.09	0.56	1.1	0.85	0.99	0.27	30	9	16048	2	55	10	1.06	4
D5B-17	m	0.02	3.1	0.09	0.91	0.74	0.53	2.7	4.6	4.2	8.2	1.8	60	40	7813	25	180	17	1.13	5
D5B-18	m	0.002	3.4	0.05	0.31	0.30	0.23	1.6	6.1	8.1	13	2.7	96	71	7707	3	231	82	1.03	13
D5B-19	m	0.008	5.5	0.10	0.68	0.60	0.49	3.4	15	27	63	14.2	165	210	6480	21	282	46	1.05	34
D5B-20	b	0.005	0.35	0.010	0.08	0.10	0.08	0.54	0.98	0.60	0.73	0.20	21	8	12657	3	43	12	0.98	3
D3F-1	m	0.005	0.19	0.006	0.08	0.07	0.07	0.47	0.82	0.62	1.1	0.26	24	7	11845	0	10	8	1.10	4
D3F-2	m	0.005	0.26	0.006	0.13	0.14	0.19	1.3	2.6	1.2	1.4	0.35	35	15	11135	1	22	11	1.34	2
D3F-3	m	0.009	0.18	0.007	0.07	0.07	0.03	0.30	1.2	2.3	4.6	0.99	43	17	10884	0	9	6	0.62	27
D3F-4	m	0.006	0.27	0.005	0.10	0.17	0.16	1.1	2.0	0.81	0.93	0.23	43	11	11558	1	26	12	1.09	2
D3F-5	m	0.11	0.39	0.02	0.09	0.14	0.11	0.89	1.4	0.96	1.3	0.27	34	10	10979	3	23	2	0.96	2
D3F-6	m	0.004	0.17	0.002	0.06	0.08	0.05	0.44	0.96	0.50	0.69	0.19	24	7	12018	0	10	16	0.90	4
D3F-7	m	0.006	0.24	0.006	0.08	0.14	0.15	1.3	2.1	1.6	2.8	0.59	46	16	11474	1	28	10	1.07	4
D3F-8	m	0.005	0.20	0.002	0.08	0.16	0.22	2.1	3.5	1.5	1.6	0.33	74	21	11102	0	26	14	1.18	1
D3F-9	m	0.009	0.38	0.03	0.30	0.20	0.15	0.78	1.6	3.1	4.8	1.0	54	25	11534	1	18	5	1.16	11
D3F-10	m	0.02	0.22	0.008	0.12	0.15	0.17	1.1	1.8	0.79	0.90	0.21	46	10	11426	1	27	4	1.26	2
D3F-11	m	0.005	0.20	0.002	0.06	0.14	0.16	1.3	2.7	0.96	1.1	0.24	36	13	11641	0	15	16	1.13	1
D3F-12	m	0.007	0.22	0.006	0.08	0.16	0.24	2.3	5.6	2.6	3.4	0.68	28	33	11882	0	23	8	1.18	2
CZ3-3.2		0.02	0.46	0.04	0.17	0.13	0.08	0.63	3.5	6.7	15	2.8	19	42	11671	25	618	4	0.82	36
CZ3-3.3		0.02	0.38	0.03	0.22	0.12	0.05	0.63	3.2	5.8	13	2.6	20	40	10635	24	591	4	0.52	33
CZ3-3.4		0.03	0.51	0.03	0.25	0.16	0.06	0.75	3.6	6.8	15	2.9	21	43	12518	27	652	4	0.50	31
CZ3-3.5		0.03	0.50	0.04	0.26	0.16	0.05	0.67	3.7	6.9	15	2.7	23	43	11530	26	637	3	0.50	33
CZ3-4.1		0.02	0.50	0.04	0.24	0.15	0.05	0.67	3.3	6.4	15	2.8	19	40	11382	24	585	4	0.47	34

TABLE 2
(*Continued*)

sample	CL	La	Ce	Pr	Nd	Sm	Eu	Gd	Dy	Er	Yb	Lu	P	Y	Hf	Th	U	Ce/ Ce*	Eu/ Eu*	Lu_n/ Gd_n
CZ3-4.2		0.02	0.44	0.04	0.23	0.14	0.05	0.66	3.2	6.3	14	2.7	18	40	10879	25	584	4	0.51	33
CZ3-4.3		0.02	0.45	0.02	0.19	0.14	0.05	0.62	3.4	6.5	15	2.6	21	41	11171	25	589	5	0.54	35
CZ3-4.4		0.02	0.43	0.03	0.19	0.13	0.04	0.70	3.2	6.0	14	2.6	20	41	10789	26	617	5	0.43	30
CZ3-4.5		0.013	0.41	0.03	0.24	0.14	0.05	0.68	3.1	6.0	13	2.5	20	40	10290	26	585	5	0.45	30
CZ3-4.6		0.011	0.45	0.02	0.30	0.19	0.05	0.66	3.6	7.0	16	2.8	19	44	11716	29	663	7	0.48	35
CZ3-4.7		0.02	0.46	0.04	0.22	0.14	0.05	0.70	3.4	6.5	15	2.6	19	43	11027	27	641	4	0.53	31
CZ3-5.1		0.02	0.43	0.03	0.22	0.13	0.05	0.58	3.2	6.2	13	2.4	22	40	9980	24	579	4	0.56	34
CZ3-5.2		0.02	0.44	0.04	0.27	0.16	0.05	0.60	3.5	6.1	14	2.7	20	41	11024	--	609	5	0.52	36
CZ3-5.2		0.009	0.41	0.02	0.24	0.12	0.05	0.57	3.2	5.6	12	2.2	19	40	9658	--	584	7	0.57	32
CZ3-5.4		0.02	0.40	0.03	0.23	0.15	0.05	0.63	3.1	5.4	12	2.3	22	40	9727	--	597	4	0.47	30
CZ3-5.5		0.011	0.38	0.03	0.19	0.10	0.04	0.57	2.8	4.9	11	2.0	20	37	9160	--	547	5	0.50	29
CZ3-5.6		0.015	0.34	0.02	0.17	0.11	0.04	0.53	2.8	4.4	10	1.8	20	37	8371	--	553	5	0.51	28
CZ3-5.7		0.007	0.36	0.02	0.16	0.13	0.04	0.55	2.8	4.7	11	1.9	21	39	8769	25	559	7	0.49	28
CZ3-5.8		0.02	0.33	0.03	0.19	0.11	0.03	0.54	2.5	4.0	8.6	1.6	21	36	7646	24	522	3	0.38	24
CZ3-6.1		0.02	0.39	0.02	0.24	0.15	0.03	0.56	2.9	4.9	11	2.1	19	38	9069	25	547	5	0.35	30
CZ3-6.2		0.013	0.37	0.02	0.16	0.13	0.04	0.62	2.9	4.9	11	2.0	18	38	8776	25	547	5	0.43	26
CZ3-6.3		0.011	0.40	0.02	0.21	0.10	0.04	0.62	2.9	4.8	11	2.1	20	39	9497	27	589	6	0.50	28
CZ3-6.4		0.02	0.41	0.02	0.16	0.12	0.05	0.68	2.8	4.6	11	2.2	23	39	9400	30	637	6	0.50	26
CZ3-6.5		0.010	0.36	0.03	0.21	0.12	0.05	0.58	3.1	5.7	12	2.4	18	38	9931	25	597	5	0.54	33
CZ3-6.6		0.02	0.40	0.02	0.24	0.13	0.05	0.71	3.5	5.8	13	2.4	20	42	11120	29	675	4	0.48	28
CZ3-7.1		0.02	0.40	0.03	0.22	0.11	0.05	0.60	3.1	5.5	12	2.3	21	40	9901	26	596	4	0.53	31
CZ3-7.2		0.013	0.37	0.02	0.22	0.12	0.04	0.63	3.0	5.2	11	2.1	18	38	9617	25	559	5	0.46	27
CZ3-7.3		0.02	0.36	0.03	0.19	0.13	0.04	0.53	2.8	4.5	10	2.0	21	37	8657	26	527	3	0.49	31
CZ3-7.4		0.02	0.44	0.03	0.23	0.15	0.05	0.73	3.5	6.7	15	2.7	19	42	11917	29	692	5	0.49	30
CZ3-8.1		0.015	0.36	0.03	0.18	0.15	0.05	0.61	2.9	5.0	12	2.2	19	39	9472	25	571	4	0.49	29
CZ3-8.2		0.02	0.38	0.03	0.17	0.12	0.05	0.61	3.1	5.7	13	2.3	22	40	10026	26	594	4	0.53	31

TABLE 2

(Continued)

sample	CL	La	Ce	Pr	Nd	Sm	Eu	Gd	Dy	Er	Yb	Lu	P	Y	Hf	Th	U	Ce/ Ce*	Eu/ Eu*	Lu_n/ Gd_n
CZ3-8.3		0.02	0.40	0.03	0.24	0.13	0.05	0.69	3.1	5.6	13	2.3	21	41	9979	26	605	4	0.47	27
CZ3-8.4		0.02	0.35	0.02	0.19	0.13	0.04	0.56	2.8	4.4	9.7	1.9	22	37	8292	26	536	4	0.42	27
CZ3-8.5		0.02	0.46	0.03	0.28	0.15	0.05	0.66	3.6	6.7	14	2.8	20	44	11547	30	683	4	0.48	34
CZ3-9.1		0.02	0.39	0.04	0.21	0.14	0.05	0.65	3.2	6.3	14	2.5	18	40	10494	24	593	3	0.54	31
CZ3-9.2		0.012	0.38	0.03	0.17	0.13	0.05	0.58	3.0	5.9	13	2.4	18	39	9783	23	547	5	0.55	33
CZ3-9.3		0.013	0.39	0.03	0.21	0.13	0.05	0.61	3.3	6.1	14	2.6	18	40	10419	24	590	5	0.59	34
CZ3-9.4		0.03	0.42	0.03	0.23	0.13	0.05	0.64	3.5	6.3	14	2.6	22	42	10868	27	627	3	0.54	33
CZ3-10.1		0.02	0.38	0.03	0.20	0.13	0.05	0.61	3.2	6.3	14	2.6	21	40	10703	24	597	4	0.51	34
CZ3-10.2		0.02	0.40	0.04	0.22	0.15	0.05	0.64	3.3	6.7	15	2.6	18	41	10852	25	584	3	0.53	33
CZ3 avg		0.02	0.41	0.03	0.21	0.13	0.05	0.63	3.2	5.7	13	2.4	20	40	10207	26	595	4.6	0.50	31
± % err		32	11	22	16	13	16	9	9	14	14	13	7	5	11	7	7	23	14	10
SL13-1.1		0.007	0.30	0.012	0.11	0.09	0.04	0.45	2.3	4.7	12	2.5	17	29	6631	15	222	8	0.59	44
SL13-1.2		0.005	0.28	0.007	0.11	0.07	0.03	0.39	2.0	4.2	11	2.3	18	28	6084	15	215	11	0.60	47
SL13-1.3		0.007	0.26	0.010	0.10	0.11	0.03	0.42	2.1	3.8	9.7	2.0	18	27	5717	15	206	7	0.42	39
SL13-1.4		0.011	0.31	0.011	0.10	0.09	0.05	0.47	2.7	5.6	15	2.9	18	32	7642	17	262	7	0.72	50
SL13-1.5		0.02	0.32	*0.02*	0.11	0.09	0.04	0.47	2.5	5.4	14	2.7	18	31	7506	17	253	4	0.63	48
SL13-2.1		0.011	0.32	0.011	0.13	0.09	0.04	0.52	2.6	5.5	14	2.8	17	32	7267	16	247	7	0.59	44
SL13 avg		0.009	0.30	0.010	0.11	0.09	0.04	0.45	2.4	4.9	13	2.5	18	30	6808	16	234	7.5	0.59	45
± % err		43	8	17	10	14	17	10	11	16	15	14	3	6	12	6	10	30	16	9

Note: Analyses performed 8–12 September 2004. Ce/Ce* = $Ce_n/(La_n * Pr_n)^{0.5}$ Eu/Eu* = $Eu_n/(Sm_n * Gd_n)^{0.5}$; the subscript indicates normalization to chondrite values of McDonough and Sun (1995). Abbreviations: b, bright CL; c, dark CL cores; d, dark CL; m, medium CL. SL13 value in italics is excluded from calculation of the average (used for calibration) and standard deviation.

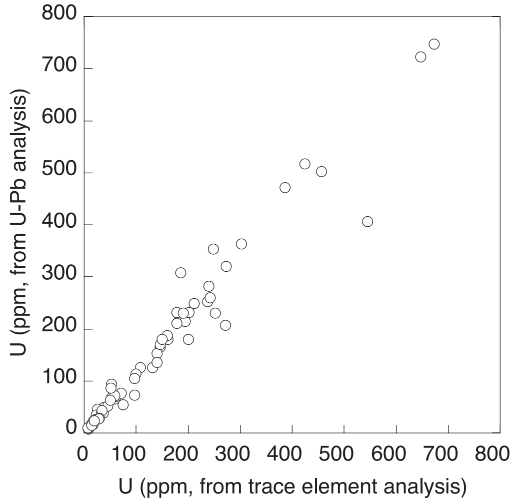

Fig. 6. Plot of U concentrations determined during U-Pb analysis (table 1) and during trace element analysis (table 2). The agreement between the two determinations suggests that U-Pb and trace element analyses sampled the same zircon zones for most analyses, and therefore the trace element data may be applied to interpret the geochronology.

Two epidote inclusions in the cores contain low Ca (fig. 9A; table 3), and EDS analysis reveals a prominent Th peak in one grain, and a prominent REE peak in the other. A garnet inclusion in a zircon rim is similar, but slightly Ca-richer than porphyroblast garnet (fig. 9B; table 3), and omphacite inclusions in zircon are compositionally identical to matrix omphacite (fig. 9C; table 3). Unlike eclogite D5A, the CL patterns of D5B do not reliably distinguish age and REE populations, and therefore the two, distinct REE patterns are used to subdivide this sample. Inclusions are too sparse to determine if systematic mineral inclusion differences exist between the two groups. Eight analyses yield relatively steep HREE patterns (Lu_n/Gd_n = 13 – 43, most analyses ~30) and lack Eu anomalies (Eu/Eu* = 1.01 – 1.15; figs. 10A and 11A; table 2). These "steep HREE" analyses yield 146 to 240 ppm U, Th/U = 0.02 – 0.24, and 419 to 459 Ma ages (figs. 10A, 10B, and 11B). A weighted mean from five analyses is 441.7 ± 4.1 Ma (MSWD = 2.2, probability = 0.061).

Ten analyses yield flat HREE patterns (Lu_n/Gd_n = 1–5) and lack Eu anomalies (Eu/Eu* = 0.93 – 1.23; figs. 10C and 11A; table 2). These "flat HREE" analyses yield 34 to 243 ppm U, Th/U = 0.03–0.25, and 421 to 445 Ma ages (figs. 10C, 10D, and 11B). A weighted mean from seven analyses is 432.5 ± 4.7 Ma (MSWD = 2.8, probability = 0.010). The bright CL, low U analyses generally correspond to the highest Hf concentrations (table 2). Two analyses (#10 and #11), one of which partially overlies a crack (#11), yielded anomalous, irregular REE patterns (table 2; not plotted in fig. 10). These analyses are interpreted to reflect modification by post crystallization alteration, and are excluded from further discussion.

Eclogite D3F

Most zircons from eclogite D3F consist of medium CL grains, or medium CL grain rims surrounding irregular, bright CL (± faint oscillatory zoning) cores (fig. 12A). Twelve analyses of the medium CL rims yield 8 to 30 ppm U, Th/U = 0.01 – 0.15, and 415 to 438 Ma ages (figs. 12A, 12B, and 11B; table 1). A weighted mean age from 10 analyses is 422.0 ± 4.3 Ma (MSWD = 0.83, probability = 0.59). The REE patterns (fig.

TABLE 3

Representative mineral compositions, North Qaidam eclogite samples D5A, D5B, and D3F

Sample	D5A	D5A	D5B	D5B	D3F	D3F	D5A	D5A	D5A	D5A	D5A	D5A
Mineral	Grt	Grt	Grt	Grt	Grt	Grt	Czo	Czo	Czo	Czo	Czo	Czo
Note	matrix	Zrn incl.	matrix	Zrn incl.	matrix	Zrn incl.	Grt incl.	Grt incl.	Grt incl.	matrix	vein	Zrn incl.
SiO_2	39.59	37.32	39.20	38.71	39.10	37.58	38.46	38.82	36.13	38.29	37.52	37.26
TiO_2	0.06	0.00	0.10	0.00	0.10	0.00	0.16	0.05	0.17	0.17	0.11	0.07
Al_2O_3	22.32	21.09	22.23	21.94	21.92	21.25	29.27	31.96	26.08	28.18	24.16	27.47
Cr_2O_3	0.07	0.00	0.04	0.00	0.04	0.00	0.11	0.12	0.32	0.02	0.07	0.00
FeO*	19.58	22.52	21.77	23.24	19.85	21.94	5.65	2.29	6.21	7.29	12.48	5.47
MnO	0.41	0.91	0.23	0.41	0.74	1.13	0.02	0.02	0.07	0.03	0.05	0.00
MgO	6.03	4.22	8.21	5.93	6.72	5.55	0.28	0.04	0.70	0.11	0.00	0.33
CaO	12.48	11.30	8.14	9.29	11.12	9.70	22.71	23.17	19.18	22.70	22.76	21.36
Na_2O	0.00	0.00	0.05	0.00	0.04	0.00	0.01	0.04	0.14	0.00	0.00	0.01
K_2O	0.00	0.00	0.00	0.00	0.00	0.00	0.02	0.02	0.00	0.00	0.01	0.00
Totals	100.54	97.46	100.01	99.53	99.66	97.21	96.68	96.52	88.98	96.81	97.17	92.57
Oxygens	12.0	12.0	12.0	12.0	12.0	12.0	12.5	12.5	12.5	12.5	12.5	12.5
Si	3.009	2.980	2.988	3.001	2.999	2.988	3.001	2.997	3.056	3.002	2.996	2.991
Ti	0.003	0.000	0.006	0.000	0.006	0.000	0.009	0.003	0.011	0.010	0.007	0.006
Al	2.000	1.985	1.997	2.005	1.982	1.992	2.692	2.909	2.600	2.605	2.274	2.950
Cr	0.004	0.000	0.003	0.000	0.003	0.000	0.007	0.007	0.021	0.001	0.005	0.003
Fe^{3+}	0.000	0.054	0.020	0.000	0.011	0.031	0.332	0.133	0.395	0.430	0.750	0.085
Fe^{2+}	1.244	1.450	1.367	1.507	1.262	1.428	0	0	0	0	0	0
Mn	0.026	0.061	0.015	0.027	0.048	0.076	0.001	0.002	0.005	0.002	0.004	0.000
Mg	0.683	0.502	0.932	0.685	0.768	0.658	0.032	0.005	0.088	0.013	0.000	0.005
Ca	1.016	0.968	0.665	0.772	0.914	0.827	1.899	1.917	1.739	1.907	1.947	1.944
Na	0.000	0.000	0.007	0.000	0.006	0.000	0.002	0.006	0.022	0.001	0.000	0.001
K	0.000	0.000	0.000	0.000	0.000	0.000	0.002	0.002	0.000	0.000	0.001	0.000
Sum	7.986	8.000	8.000	7.997	8.000	8.000	7.976	7.979	7.937	7.971	7.983	7.985

Table 3

(Continued)

Sample	D5B	D3F	D5A	D5A	D5B	D5B	D3F	D5A	D5A	D3F	D3F	D5A	D5A
Mineral	Czo	Czo	Cpx	Cpx	Cpx	Cpx	Cpx	Amp	Amp	Amp	Amp	Pl	Pl
Note	Zrn incl.	Grt incl.	matrix	symp.	matrix	Zrn incl.	Zrn incl.	matrix	vein	Grt incl.	Grt incl.	symp.	vein
SiO_2	33.31	39.35	55.92	53.59	55.34	55.74	55.00	45.14	41.57	49.43	43.95	64.96	64.86
TiO_2	0.05	0.10	0.24	0.14	0.10	0.00	0.00	0.37	0.18	0.33	0.44	0.03	0.03
Al_2O_3	22.26	32.93	11.72	3.59	8.20	7.87	7.83	14.86	12.62	11.92	17.54	22.03	21.79
Cr_2O_3	0.25	0.05	0.02	0.08	0.08	0.00	0.03	0.03	0.02	0.02	0.08	0.01	0.04
FeO*	7.59	1.49	4.78	6.75	4.55	4.10	2.48	10.34	15.11	7.03	8.48	0.19	0.17
MnO	0.01	0.00	0.04	0.06	0.00	0.00	0.00	0.06	0.18	0.04	0.02	0.04	0.01
MgO	1.26	0.05	7.73	12.49	10.19	10.43	11.59	12.62	11.90	15.50	12.61	0.01	0.00
CaO	17.13	23.87	12.75	20.78	15.90	15.99	17.65	8.20	11.72	9.82	10.35	2.96	2.50
Na_2O	0.12	0.01	7.14	2.36	5.40	5.18	4.22	5.00	3.12	2.42	2.77	10.34	10.28
K_2O	0.00	0.00	0.00	0.00	0.00	0.00	0.00	0.24	0.25	0.33	0.17	0.01	0.00
Totals	81.98	97.84	100.35	99.82	99.75	99.31	98.80	97.06	97.09	97.04	96.61	100.58	99.68
Oxygens	12.5	12.5	6.0	6.0	6.0	6.0	6.0	23.0	23.0	23.0	23.0	8.0	8.0
Si	3.049	3.078	1.980	1.964	1.983	2.006	1.988	6.520	6.225	6.961	6.311	2.849	2.864
Ti	0.004	0.004	0.006	0.004	0.003	0.000	0.000	0.040	0.020	0.035	0.048	0.001	0.001
Al	2.650	2.425	0.489	0.155	0.346	0.334	0.333	2.530	2.228	1.979	2.969	1.139	1.134
Cr	0.000	0.018	0.001	0.002	0.002	0.000	0.001	0.003	0.003	0.003	0.009	0.000	0.001
Fe^{3+}	0.337	0.528	0.000	0.010	0.026	0.027	0.000	0.232	0.473	0.219	0.200	0.006	0.006
Fe^{2+}	0	0	0.141	0.196	0.110	0.096	0.075	1.017	1.418	0.608	0.818	0	0
Mn	0.000	0.001	0.001	0.002	0.000	0.000	0.000	0.007	0.023	0.004	0.003	0.001	0.000
Mg	0.040	0.174	0.408	0.682	0.544	0.559	0.624	2.717	2.656	3.253	2.699	0.001	0.000
Ca	1.873	1.696	0.484	0.816	0.610	0.617	0.683	1.269	1.881	1.482	1.593	0.139	0.118
Na	0.002	0.021	0.490	0.168	0.375	0.361	0.295	1.401	0.907	0.660	0.772	0.879	0.880
K	0.000	0.000	0.000	0.000	0.000	0.000	0.000	0.044	0.048	0.059	0.032	0.000	0.000
Sum	7.955	7.944	4.000	4.000	4.000	4.000	4.000	15.780	15.881	15.263	15.454	5.017	5.005

Note: Ferric iron estimated for garnet (Droop, 1987 technique, 8 cations, 12 oxygens); for clinozoisite (all ferric); for clinopyroxene (Na-Al-Cr); for amphibole (average of maximum and minimum constraints after Leake and others, 1997), for plagioclase (all ferric).

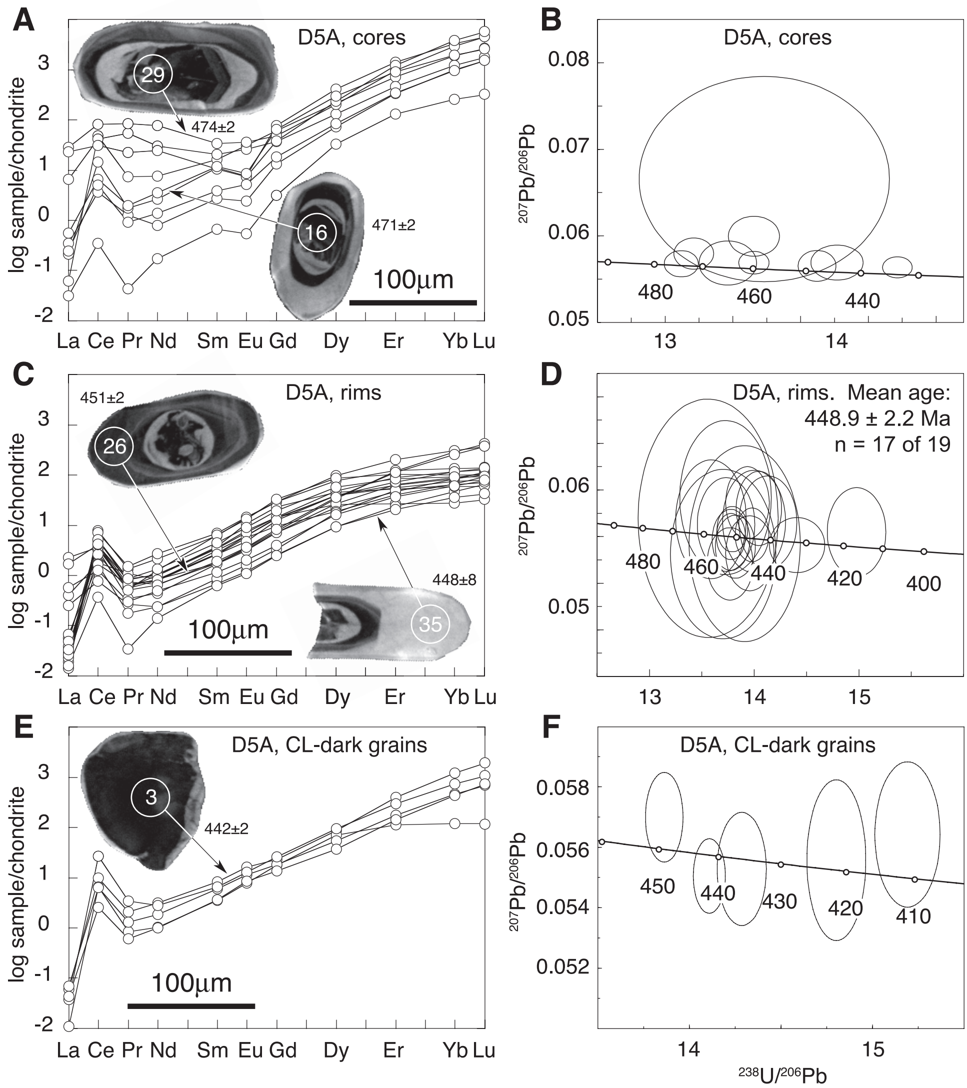

Fig. 7. (A, C, E) Cathodoluminescence (CL) images and REE patterns (Coryell and others, 1963) normalized to chondrite values of McDonough and Sun (1995) for eclogite D5A zircon cores (A), rims (C), and CL dark grains (E). Circles show the locations of ~30 μm SHRIMP-RG analyses, labeled with their analysis number (tables 1 and 2) and ^{207}Pb-corrected ^{206}Pb/^{238}U age (Williams, 1998), and 1σ error. (B, D, F) Tera-Wasserburg concordia (Tera and Wasserburg, 1972) for eclogite D5A zircon cores (B), rims (D), and CL dark grains (F). Plotted ratios are uncorrected for common Pb, and error ellipses are 2σ.

12A) are characterized by flat HREE slopes (Lu_n/Gd_n = 1 – 11) and lack Eu anomalies (Eu/Eu* = 0.90 – 1.34; figs. 12A and 11A; table 2). One analysis (#3) excluded from the weighted mean age has a steeper HREE slope (Lu_n/Gd_n = 27), a small Eu anomaly (Eu/Eu* = 0.62), and an older age (435 ± 13 Ma) than the other analyses, and reflects partial overlap on a brighter CL core. No analyses of the bright CL cores were performed due to extremely low U concentrations. The zircons contain inclusions of garnet, omphacite, and rutile in both bright CL and medium CL domains. Composi-

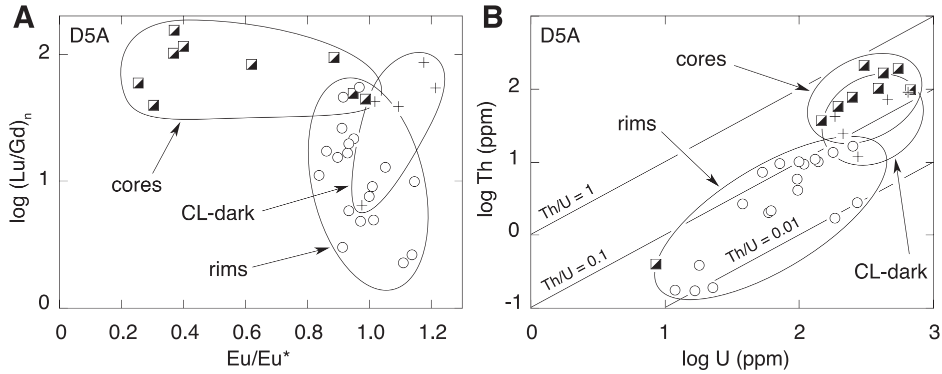

Fig. 8. (A) Plot of HREE slope [log $(Lu/Gd)_n$] against Eu anomaly [$Eu/Eu^* = Eu_n/(Sm_n \times Gd_n)^{0.5}$] for eclogite D5A zircons. (B) Th and U concentration data determined during U-Pb geochronology (table 1) for eclogite D5A zircons.

tions of garnet inclusions are similar to, but slightly iron-richer than compositions of garnet porphyroblasts (fig. 9B; table 3).

Eclogite D3G

Zircons from eclogite D3G have similar CL patterns to eclogite D3F, but bright CL cores are more common. Eight analyses of medium CL rims yielded 1 to 13 ppm U, Th/U = 0.01 – 0.05, and 356 to 450 Ma ages with large uncertainties due to the extremely low U concentrations and resulting high proportion of common Pb (table 1). This sample does not provide useful additional age constraints, and therefore no trace element analyses were performed. The zircons contain sparse inclusions of rutile, omphacite, and garnet.

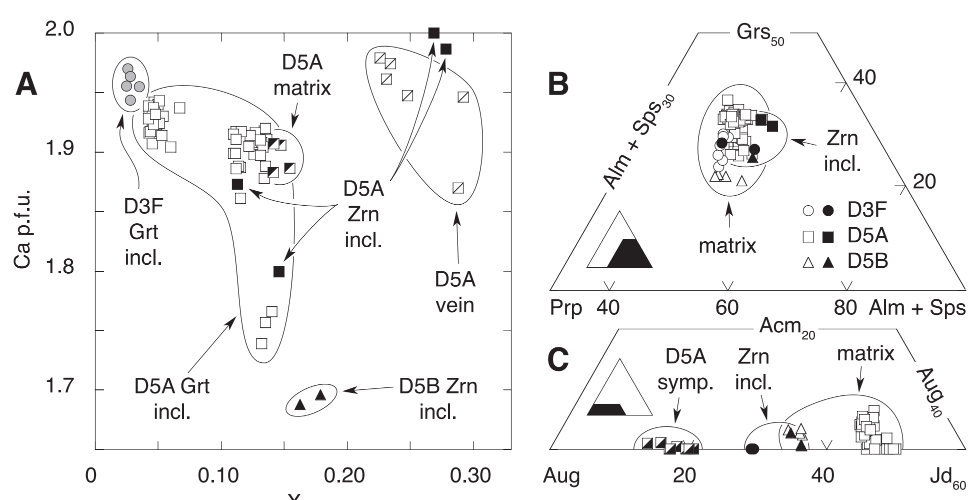

Fig. 9. Compositions of matrix and inclusion (incl.) minerals determined by electron microprobe. (A) Epidote compositions based on 12.5 O per formula unit (p.f.u.); $X_{Fe} = Fe/(Fe + Al)$, all Fe assumed ferric. (B) Eclogite garnet compositions. Open symbols are matrix analyses, and filled symbols are zircon inclusions. (C) Eclogite omphacite compositions (symbols as in B). Ferric iron is estimated from Na - Al - Cr. Mineral abbreviations follow Kretz (1983).

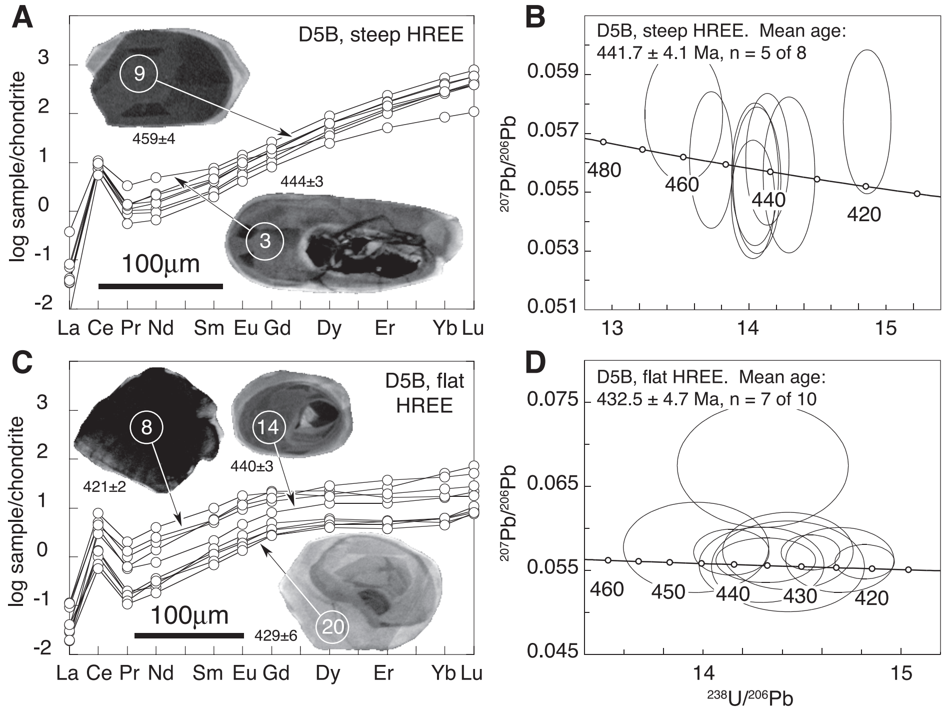

Fig. 10. (A, C) Cathodoluminescence (CL) images and REE patterns (Coryell and others, 1963) normalized to chondrite values of McDonough and Sun (1995) for garnet-rich eclogite D5B zircon steep HREE analyses (A), and flat HREE analyses (C). Circles show the locations of ~30 μm SHRIMP-RG analyses, labeled with their analysis number (tables 1 and 2) and ^{207}Pb-corrected $^{206}Pb/^{238}U$ age (Williams, 1998), and 1σ error. (B, D) Tera-Wasserburg concordia (Tera and Wasserburg, 1972) for garnet-rich eclogite D5B zircon steep HREE analyses (B), and flat HREE analyses (D). Plotted ratios are uncorrected for common Pb, and error ellipses are 2σ.

DISCUSSION

The eclogite D5A rims, D5B flat HREE analyses, and D3F record an ~25 m.y. range of weighted mean ages (fig. 13; table 1). Zircons from each of these samples

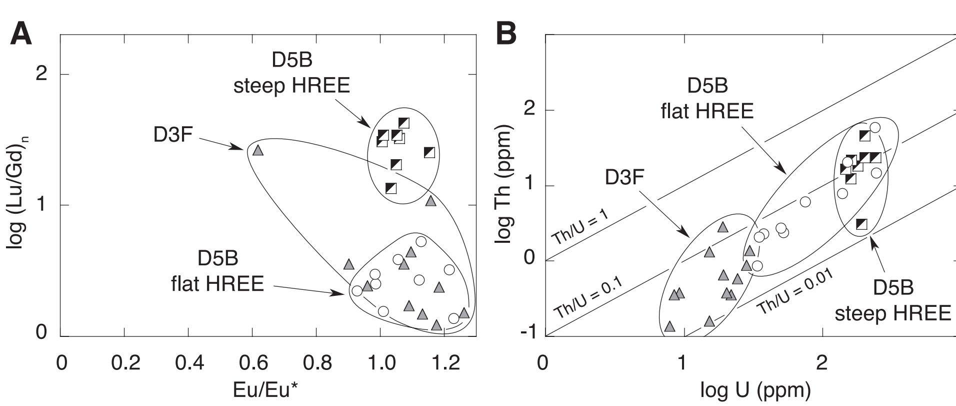

Fig. 11. (A) Plot of HREE slope [log $(Lu/Gd)_n$] against Eu anomaly [$Eu/Eu^* = Eu_n/(Sm_n \times Gd_n)^{0.5}$] for eclogite D5B and D3F zircons. (B) Th and U concentration data determined during U-Pb geochronology (table 1) for eclogite D5B and D3F zircons.

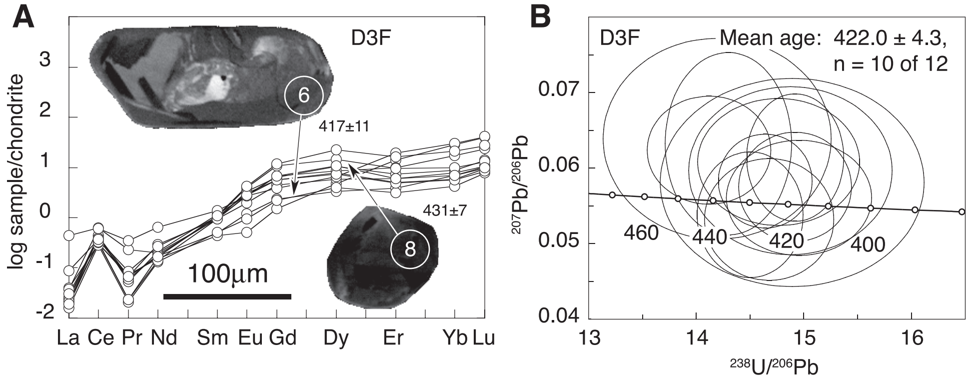

Fig. 12. (A) Cathodoluminescence (CL) images and REE patterns (Coryell and others, 1963) normalized to chondrite values of McDonough and Sun (1995) for eclogite D3F. Circles show the locations of ~30 µm SHRIMP-RG analyses, labeled with their analysis number (tables 1 and 2) and ^{207}Pb-corrected ^{206}Pb/^{238}U age (Williams, 1998), and 1σ error. (B) Tera-Wasserburg concordia (Tera and Wasserburg, 1972) for eclogite D3F. Plotted ratios are uncorrected for common Pb, and error ellipses are 2σ.

contain garnet, omphacite, and rutile, suggesting eclogite-facies zircon growth. The similarity between compositions of garnet and omphacite inclusions in zircon, and garnet and omphacite in the matrix of the samples (figs. 9A and 9B; table 3) is consistent with zircon growth during crystallization of the mineral assemblage observed in thin section. The REE patterns also indicate that zircons grew in the eclogite-facies: the absence of Eu anomalies suggests that plagioclase was absent, and the flat HREE patterns suggest that significant garnet growth competed for HREE (Rubatto, 2002; Rubatto and Hermann, 2003). This is particularly evident in zircons from garnet-rich eclogite D5B that have lower HREE concentrations than D5A zircons (figs. 8C and 10C), consistent with consumption of HREE by garnet.

The range of ages may reflect: (1) each sample recorded a discrete event, and that subsequently the samples were juxtaposed, or (2) that all samples experienced similar conditions, but that zircon growth occurred at different times in the different samples

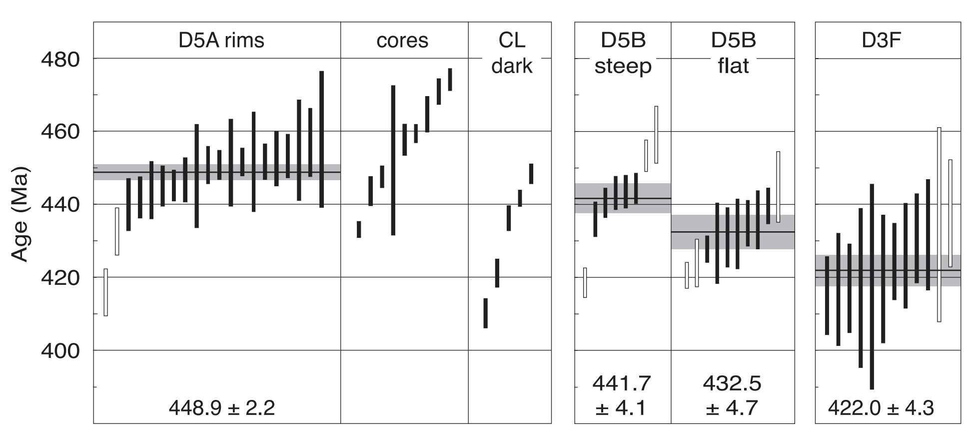

Fig. 13. Geochronology summary diagram for eclogites D5A, D5B, and D3F. Bars represent ^{207}Pb-corrected ^{206}Pb/^{238}U ages (Williams, 1998), and bar heights represent 2σ errors. Heavy horizontal lines represent weighted mean ages listed at the bottom of the diagram, and gray bands indicate 2σ errors. Unfilled bars represent analyses excluded from the weighted mean age calculation.

during protracted residence at eclogite-facies conditions. The close proximity of the samples (fig. 2) and the absence of evidence for a major structure separating them argues against the first possibility. Another observation which supports the second possibility is that although the samples have distinctly different mean ages, the range of ages recorded in each sample is similar (fig. 13; except for the older cores in D5A), which is consistent with an extended residence at eclogite-facies conditions. The reasons for episodic zircon growth during prolonged metamorphism are unconstrained by this study, but likely include the role of spatially and temporally heterogeneous fluid flow in promoting recrystallization (for example, Austrheim, 1987) and Zr-releasing mineral reactions (for example, Rubin and others, 1993; Fraser and others, 1997; Pan, 1997; Bingen and others, 2001), and may also include complex P-T-t paths (for example, Stöckhert and Gerya, 2005).

Preexisting zircon is usually the most significant source of Zr for new zircon growth during metamorphism (Rubatto and Hermann, 2003), but relict magmatic zircon appears to be absent from D5A. The cores in sample D5A contain REE patterns similar to those found in many igneous and metamorphic environments (for example, Hoskin and Ireland, 2000), but in combination with the inclusions of epidote, rutile, and garnet suggest that the zircons grew during metamorphism in a high P/T environment, and are not magmatic relics from the eclogite protolith. Although this metamorphism need not have occurred during the same event that produced the eclogite-facies assemblage, this is the simplest explanation and seems best in accord with the small difference in age between cores and rims.

The significance of the CL dark, steep HREE analyses in sample D5A is unclear. In addition to the distinctive REE patterns, the scarcity of inclusions and the grain aggregate morphology distinguish these from the other grains. The REE patterns are similar to the steep HREE D5B grains, but the D5B grains do not share the aggregate morphology, and are on average older than the eclogite-facies grains (fig. 13), whereas the D5A CL dark grains yield scattered but generally younger ages relative to the eclogite-facies rims (fig. 13).

The steep HREE analyses in garnet-rich eclogite D5B lack an Eu anomaly, suggesting the absence of plagioclase, but the steep HREE patterns ($Lu_n/Gd_n \approx 30$) are intermediate between the D5A core analyses ($Lu_n/Gd_n \approx 90$) and the eclogite-facies rims of all three samples ($Lu_n/Gd_n = 1 - 10$), suggesting the absence of abundant garnet. This contrasts with the garnet-rich assemblage observed in thin section, which seems in accord with the flat HREE analyses. One possibility is that the steep HREE zircon grains grew prior to most of the garnet, which is also consistent with the generally older ages of the steep HREE analyses. Intriguingly, the ca. 10 m.y. duration of garnet growth implied by this hypothesis is in good agreement with the 10 to 20 m.y. garnet growth durations recently determined from UHP eclogite in the Alps (Lapen and others, 2003) and Norway (Kylander-Clark and others, 2005). A possible test of this suggestion would be to examine garnet core REE compositions for equilibrium with steep HREE zircon (for example, Rubatto, 2002; Hermann and Rubatto, 2003; Whitehouse and Platt, 2003; Kelly and Harley, 2005).

The composition and blocky shape of the polycrystalline clinozoisite inclusions in the cores of garnets (figs. 4A – 4D) suggests they may represent lawsonite pseudomorphs. Kyanite, mica, or omphacite, which are commonly associated with lawsonite decomposition (for example, Newton and Kennedy, 1963; Okrusch and others, 1978; Forbes and others, 1984; Tribuzio and others, 1996; Schulte and Sindern, 2002; Beane and Liou, 2005) are absent, although some inclusions contain amphibole adjacent to or intergrown with clinozoisite (fig. 4D). However, examples of lawsonite pseudomorphs largely or completely composed of zoisite or clinozoisite are also known (for example, Krogh, 1982; Helmstaedt and Schultze, 1988; Pognante, 1989; Usui and others, 2003, 2006; Zack and others, 2004). Clinozoisite in the inclusions includes both low-Fe (X_{Fe} = 0.05) and intermediate Fe (X_{Fe} = 0.12–0.14) compositions (figs. 4B and 9A; table 3), which suggests a miscibility gap. Inclined extinction of one of the low-Fe grains indicates that this compositional gap separates two different clinozoisites (for example, Gottschalk, 2004, p. 119) rather than zoisite and clinozoisite. In BSE, bright grain cores (figs. 4A and 4B) correspond to low Ca compositions (fig. 9A), and EDS analysis indicates the presence of REE, which would be expected to partition into epidote minerals during lawsonite decomposition (for example, Tribuzio and others, 1996; Spandler and others, 2003; Sr was not analyzed but may be present as well). The rims of the garnet, but not the cores, contain tiny inclusions of a Ba, Sr, S mineral, probably (Ba, Sr)SO_4 (fig. 4A; O is not detectable by EDS). The release of Ba and Sr to form these minerals would be expected during lawsonite breakdown (for example, Tribuzio and others, 1996; Spandler and others, 2003).

The interpretation of these inclusions as lawsonite pseudomorphs implies a cold, prograde subduction path for the UHP rocks (for example, Poli and Schmidt, 1995). The breakdown of lawsonite to form clinozoisite should result in significant fluid release, which may have catalyzed the growth of zircon (for example, Usui and others, 2003). The compositional similarity of two clinozoisite inclusions in zircon to clinozoisite included in garnet (fig. 9A) is consistent with this hypothesis, but could also indicate that allanite decomposition contributed to zircon formation (for example, Pan, 1997).

The 449 to 422 Ma ages of eclogite-facies metamorphism obtained in this study are slightly younger than the 458 ± 10 Ma and 459 ± 3 Ma Sm-Nd isochron ages and the 457 ± 7 Ma zircon age reported by Song and others (2003a, 2006) for eclogites from this area. One possible explanation is that the Sm-Nd analyses may average prograde and peak-stage garnet, resulting in a bias toward older ages (for example, Carswell and others, 2003). The isochrons reported by Song and others (2003a) are effectively 2-point isochrons with the age resolution controlled by garnet, due to the near-coincidence of the omphacite and whole-rock analyses. We observe that garnet in most eclogites of the Dulan region contain prograde inclusions in their cores, and therefore these analyses may be influenced by prograde garnet. Another possibility for the age discrepancy, supported by the zircon age reported by Song and others (2006) is that the eclogites analyzed by Song and others (2003a, 2006) recrystallized earlier than the eclogites examined in this study, and therefore the age range has geologic significance.

Approximately 350 km further west in the North Qaidam terrane, zircon geochronology of eclogite from the Lüliang Shan (fig. 1) yields ages of 495 to 488 Ma (Yang and others, 2001b; Zhang and others, 2005b), and garnet peridotite records ages from zircon cores of 484 to 444 Ma, and ages from zircon mantles of 435 to 414 Ma interpreted to record UHP metamorphism (Song and others, 2005). The age range recorded by the Lüliang Shan peridotite is similar to that for the Dulan eclogites examined in this study (fig. 13), and suggests that this locality also records evidence compatible with prolonged residence at eclogite-facies conditions.

The absence of a correlation between young ages and high U concentrations (table 1) suggests that radiation damage-related Pb loss is not responsible for the age range observed in the studied eclogites (fig. 13). Ages form distinct clusters, and lack the correlation between young ages and excess scatter expected for Pb loss. Except as noted above, CL images and REE patterns do not suggest that these ages represent mixtures of different growth zones, and therefore we conclude that these ages reliably reflect the age and duration of zircon growth. The 423 ± 6 Ma zircon U-Pb age for coesite-bearing paragneiss (Song and others, 2006) is identical to the 422 ± 5 Ma age of the youngest eclogite reported in this study, which suggests that the ~25 m.y. duration of eclogite-facies metamorphism reflects the prograde path.

If these data are used to calculate an average vertical sinking rate assuming a coherent, continuously moving slab, as is commonly used in models of UHP metamorphism (for example, Chemenda and others, 1996; Ernst and others, 1997), the resulting rates (2 – 4 mm/a) are far slower than known modern subduction rates (12 – 62 mm/a vertical component; Cross and Pilger, 1982; DeMets, 1990; Calvert, 2004; England and others, 2004). This suggests that the UHP rocks did not remain fully coupled to the subducting slab throughout eclogite-facies metamorphism, but additional geochronology and thermobarometry are needed to better constrain this part of the geological history. The minimum exhumation rate is poorly constrained to >3 – 6 mm/a by a 403 ± 9 Ma zircon overgrowth and a 402 ± 2 Ma $^{40}Ar/^{39}Ar$ plateau age interpreted to reflect retrogression and cooling (Song and others, 2006), and by the 397 ± 3 Ma age of the cross-cutting Yematan batholith (Wu and others, 2004). Depositionally overlying Devonian sediments (BGMQ, 1991) indicate that the UHP rocks were exposed at the surface by ~360 Ma, as is also observed in the Lüliang Shan 350 km to the west (Menold and others, 2004, 2005).

The metamorphic age range observed in this study is similar to ranges in other UHP terranes revealed by a growing base of high-quality geochronology. For example, McClelland and others (2006) report zircon U-Pb ages coupled with REE and Raman analysis of zircon inclusions which they interpret to reflect residence of the Northeast Greenland eclogite province at eclogite-facies conditions for 30 to 50 m.y. Combined Lu-Hf and Sm-Nd geochronology reveals 10 to 20 m.y. of eclogitic garnet growth in the Alps (Lapen and others, 2003) and Norway (Kylander-Clark and others, 2005). A compilation of U-Pb, Sm-Nd, and Rb-Sr ages from the Dabie and Sulu UHP terranes reported by Leech and others (2006) reveals a ca. 30 m.y. age range for both Dabie and Sulu, and may also reflect an extended high-pressure history.

These long eclogite-facies residence times (10s of m.y.) contrast with shorter eclogite-facies durations documented from other localities (for example, Liati and Gebauer, 1999; Baldwin and others, 2004, 2005; Leech and others, 2005) and may reflect the processes operating during HP/UHP metamorphism in different tectonic settings (Searle and others, 2001; Stöckhert and Gerya, 2005; McClelland and others, 2006). The differences in geologic setting responsible for variable eclogite-facies durations remain to be explored, but we note that UHP metamorphism which occurs near the beginning of a collisional event (for example, the Himalaya: Leech and others, 2005; Papua New Guinea: Baldwin and others, 2004, 2005) is associated with shorter eclogite-facies durations than UHP metamorphism which occurs near the end of a collisional event (for example, Greenland: McClelland and others, 2006; Norway: Kylander-Clark and others, 2005; North Qaidam: this study; Menold and others, 2004, 2005; Song and others, 2006). In the North Qaidam terrane, evidence for prolonged eclogite-facies metamorphism is preserved in both the Dulan region and the Lüliang Shan, indicating that the Dulan region is not an anomaly, and that the processes responsible for extended high-pressure residence operated over a distance of 350 km along strike. Evidence of prolonged eclogite-facies metamorphism in several other HP/UHP localities (listed above) suggests long eclogite-facies residence may be globally significant in continental subduction/collision zones.

ACKNOWLEDGMENTS

We thank A. Bian and S. Y. Chen for assistance in the field, F. K. Mazdab for assistance with the development of the SHRIMP-RG trace element analysis technique, B. Wiegand, J. R. Metcalf, T. Tsujimori, and M. Vogel for assistance with the SHRIMP-RG analyses, and W. G. Ernst for constructive comments on a preliminary version of this manuscript. Careful reviews by G. Gehrels and an anonymous reviewer significantly improved the manuscript. This research was supported by grants from Stanford

University and the Geological Society of America (Grant #7466-03) to C. G. Mattinson, and a grant from the National Science Foundation (NSF-EAR0408690) to D. K. Bird.

References

Amato, J. M., Johnson, C. M., Baumgartner, L. P., and Beard, B. L., 1999, Rapid exhumation of the Zermatt–Saas ophiolite deduced from high-precision Sm–Nd and Rb–Sr geochronology: Earth and Planetary Science Letters, v. 171, p. 425–438.

Baldwin, S. L., Monteleone, B. D., Webb, L. E., Fitzgerald, P. G., Grove, M., and Hill, E. J., 2004, Pliocene eclogite exhumation at plate tectonic rates in eastern Papua New Guinea: Nature, v. 431, p. 263–267.

Baldwin, S. L., Webb, L. E., and Monteleone, B. D., 2005, Late Miocene-Pliocene eclogites of eastern Papua New Guinea: The youngest known HP/UHP terrane on earth: Mitteilungen der Österreichischen Geologischen Gesellschaft, v. 150, p. 16.

Beane, R. J., and Liou, J. G., 2005, Metasomatism in serpentinite mélange rocks from the high-pressure Maksyutov Complex, southern Ural Mountains, Russia: International Geology Review, v. 47, p. 24–40.

Bingen, B., Davis, W. J., and Austrheim, H., 2001, Zircon U-Pb geochronology in the Bergen arc eclogites and their Proterozoic protoliths, and implications for the pre-Scandian evolution of the Caledonides in western Norway: Geological Society of America Bulletin, v. 113, p. 640–649.

Black, L. P., Kamo, S. L., Allen, C. M., Davis, D. W., Aleinikoff, J. N., Valley, J. W., Mundil, R., Campbell, I. H., Korsch, R. J., Williams, I. S., and Foudoulis, C., 2004, Improved $^{206}Pb/^{238}U$ microprobe geochronology by the monitoring of a trace-element-related matrix effect; SHRIMP, ID-TIMS, ELA-ICP-MS and oxygen isotope documentation for a series of zircon standards: Chemical Geology, v. 205, p. 115–140.

Brueckner, H. K., and Van Roermund, H. L. M., 2004, Dunk tectonics: A multiple subduction/eduction model for the evolution of the Scandinavian Caledonides: Tectonics, v. 23, TC2004, doi:10.1029/2003TC001502.

Bureau of Geology and Mineral Resources of Qinghai Province (BGMQ), 1991, Regional Geology of Qinghai Province: Beijing, Geological Publishing House, Geological Memoirs, v. 24, 662 p., (in Chinese with English abstract).

Calvert, A. J., 2004, Seismic reflection imaging of two megathrust shear zones in the northern Cascadia subduction zone: Nature, v. 428, p. 163–167.

Carswell, D. A., Brueckner, H. K., Cuthbert, S. J., Mehta, K., and O'Brien, P. J., 2003, The timing of stabilisation and the exhumation rate for ultra-high pressure rocks in the Western Gneiss Region of Norway: Journal of Metamorphic Geology, v. 21, p. 601–612.

Chemenda, A. I., Mattauer, M., and Bokun, A. N., 1996, Continental subduction and a mechanism for exhumation of high-pressure metamorphic rocks: new modelling and field data from Oman: Earth and Planetary Science Letters, v. 143, p. 173–182.

Chopin, C., 1984, Coesite and pure pyrope in high-grade blueschists of the western Alps: a first record and some consequences: Contributions to Mineralogy and Petrology, v. 86, p. 107–118.

Cong, B., Wang, Q., and Zhai, M., 2000, New data regarding hotly debated topics concerning UHP metamorphism of the Dabie-Sulu belt, east-central China, *in* Ernst, W. G., and Liou, J. G., editors, Ultra-high pressure metamorphism and geodynamics in collision-type orogenic belts: Columbia, Bellwether Publishing, p. 181–189.

Coryell, C. D., Chase, J. W., and Winchester, J. W., 1963, A procedure for geochemical interpretation of terrestrial rare-earth abundance patterns: Journal of Geophysical Research, v. 68, p. 559–566.

Cross, T. A., and Pilger, R. H., Jr., 1982, Controls of subduction geometry, location of magmatic arcs, and tectonics of arc and back-arc regions: Geological Society of America Bulletin, v. 93, p. 545–562.

de Jong, K., 2003, Very fast exhumation of high-pressure metamorphic rocks with excess ^{40}Ar and inherited ^{87}Sr, Betic Cordilleras, southern Spain: Lithos, v. 70, p. 91–110.

DeMets, C., Gordon, R. G., Argus, D. F., and Stein, S., 1990, Current plate motions: Geophysical Journal International, v. 101, p. 425–478.

Droop, G. T. R., 1987, A general equation for estimating Fe^{3+} concentrations in ferromagnesian silicates and oxides from microprobe analyses, using stoichiometric criteria: Mineralogical Magazine, v. 51, p. 431–435.

England, P., Engdahl, R., and Thatcher, W., 2004, Systematic variation in the depths of slabs beneath arc volcanoes: Geophysical Journal International, v. 156, p. 377–408.

Ernst, W. G., Maruyama, S., and Wallis, S., 1997, Buoyancy-driven, rapid exhumation of ultrahigh-pressure metamorphosed continental crust: Proceedings of the National Academy of Sciences of the United States of America, v. 94, p. 9532–9537.

Forbes, R. B., Evans, B. W., and Thurston, S. P., 1984, Regional progressive high-pressure metamorphism, Seward Peninsula, Alaska: Journal of Metamorphic Geology, v. 2, p. 43–54.

Fraser, G., Ellis, D., and Eggins, S., 1997, Zirconium abundance in granulite-facies minerals, with implications for zircon geochronology in high-grade rocks: Geology, v. 25, p. 607–610.

Gebauer, D., Schertl, H. P., Brix, M., and Schreyer, W., 1997, 35 Ma old ultrahigh-pressure metamorphism and evidence for very rapid exhumation in the Dora Maira Massif, Western Alps: Lithos, v. 41, p. 5–24.

Gehrels, G. E., Yin, A., and Wang, X. F., 2003a, Detrital-zircon geochronology of the northeastern Tibetan plateau: Geological Society of America Bulletin, v. 115, p. 881–896.

——— 2003b, Magmatic history of the northeastern Tibetan Plateau: Journal of Geophysical Research, v. 108, 2423, doi:10.1029/2002JB001876.

Gottschalk, M., 2004, Thermodynamic properties of zoisite, clinozoisite and epidote: Reviews in Mineralogy and Geochemistry, v. 56, p. 83–124.

Hacker, B. R., and Gans, P. B., 2005, Continental collisions and the creation of ultrahigh-pressure terranes: Petrology and thermochronology of nappes in the central Scandinavian Caledonides: Geological Society of America Bulletin, v. 117, p. 117–134.

Hacker, B. R., and Peacock, S. M., 1995, Creation, preservation, and exhumation of UHPM rocks, *in* Coleman, R. G., and Wang, X., editors, Ultrahigh Pressure Metamorphism: New York, Cambridge University Press, p. 159–181.

Hacker, B. R., Ratschbacher, L., Webb, L., McWilliams, M. O., Ireland, T., Calvert, A., Dong, S., Wenk, H. R., and Chateigner, D., 2000, Exhumation of ultrahigh-pressure continental crust in east central China: Late Triassic-Early Jurassic tectonic unroofing: Journal of Geophysical Research, v. 105, p. 13339–13364.

Hacker, B. R., Andersen, T. B., Root, D. B., Mehl, L., Mattinson, J. M., and Wooden, J. L., 2003a, Exhumation of high-pressure rocks beneath the Solund Basin, Western Gneiss Region of Norway: Journal of Metamorphic Geology, v. 21, p. 613-629.

Hacker, B. R., Calvert, A., Zhang, R. Y., Ernst, W. G., and Liou, J. G., 2003b, Ultrarapid exhumation of ultrahigh-pressure diamond-bearing metasedimentary rocks of the Kokchetav Massif, Kazakhstan?: Lithos, v. 70, p. 61–75.

Helmstaedt, H., and Schulze, D. J., 1988, Eclogite-facies ultramafic xenoliths from Colorado Plateau diatreme breccias: Comparison with eclogites in crustal environments, evaluation of the subduction hypothesis, and implications for eclogite xenoliths from diamondiferous kimberlites, *in* Smith, D. C., editor, Eclogites and Eclogite-Facies Rocks: Amsterdam, Elsevier, p. 387–450.

Hermann, J., and Rubatto, D., 2003, Relating zircon and monazite domains to garnet growth zones: age and duration of granulite facies metamorphism in the Val Malenco lower crust: Journal of Metamorphic Geology, v. 21, p. 833–852.

Hermann, J., Rubatto, D., Korsakov, A., and Shatsky, V. S., 2001, Multiple zircon growth during fast exhumation of diamondiferous, deeply subducted continental crust (Kokchetav Massif, Kazakhstan): Contributions to Mineralogy and Petrology, v. 141, p. 66–82.

Hoskin, P. W. O., 1998, Minor and trace element analysis of natural zircon ($ZrSiO_4$) by SIMS and laser ablation ICPMS: A consideration and comparison of two broadly competitive techniques: Journal of Trace and Microprobe Techniques, v. 16, p. 301–326.

Hoskin, P. W. O., and Ireland, T. R., 2000, Rare earth element chemistry of zircon and its use as a provenance indicator: Geology, v. 28, p. 627–630.

Kaneko, Y., Katayama, I., Yamamoto, H., Misawa, K., Ishikawa, M., Rehman, H. U., Kausar, A. B., and Shiraishi, K., 2003, Timing of Himalayan ultrahigh-pressure metamorphism: sinking rate and subduction angle of the Indian continental crust beneath Asia: Journal of Metamorphic Geology, v. 21, p. 589–599.

Kelly, N. M., and Harley, S. L., 2005, An integrated microtextural and chemical approach to zircon geochronology: refining the Archaean history of the Napier Complex, east Antarctica: Contributions to Mineralogy and Petrology, v. 149, p. 57–84.

Kretz, R., 1983, Symbols for rock-forming minerals: American Mineralogist, v. 68, p. 277–279.

Krogh, E. J., 1982, Metamorphic evolution of Norwegian country-rock eclogites, as deduced from mineral inclusions and compositional zoning in garnets: Lithos, v. 15, p. 305–321.

Kylander-Clark, A., Hacker, B., Johnson, C., Beard, B., Mahlen, N., and Lapen, T., 2005, Lu/Hf and Sm/Nd ages of eclogite-facies metamorphism in the Western Gneiss Region, Norway: Geological Society of America Abstracts with Programs, v. 37, p. 390.

Lapen, T. J., Johnson, C. M., Baumgartner, L. P., Mahlen, N. J., Beard, B. L., and Amato, J. M., 2003, Burial rates during prograde metamorphism of an ultra-high-pressure terrane: an example from Lago di Cignana, western Alps, Italy: Earth and Planetary Science Letters, v. 215, p. 57–72.

Leake, B. E., Woolley, A. R., Arps, C. E. S., Birch, W. D., Gilbert, M. C., Grice, J. D., Hawthorne, F. C., Kato, A., Kisch, H. J., Krivovichev, V. G., Linthout, K., Laird, J., Mandarino, J. A., Maresch, W. V., Nickel, E. H., Rock, N. M. H., Schumacher, J. C., Smith, D. C., Stephenson, N. C. N., Ungaretti, L., Whittaker, E. J. W., and Youzhi, G., 1997, Nomenclature of amphiboles: Report of the Subcommittee on Amphiboles of the International Mineralogical Association, Commission on New Minerals and Mineral Names: American Mineralogist, v. 82, p. 1019–1037.

Leech, M. L., Singh, S., Jain, A. K., Klemperer, S. L., and Manickavasagam, R. M., 2005, The onset of India–Asia continental collision: Early, steep subduction required by the timing of UHP metamorphism in the western Himalaya: Earth and Planetary Science Letters, v. 234, p. 83–97.

Leech, M. L., Webb, L. E., and Yang, T. N., 2006, Diachronous histories for the Dabie-Sulu orogen from high-temperature geochronology, *in* Hacker, B. R., McClelland, W. C., and Liou, J. G., editors, Ultrahigh-pressure metamorphism: Deep continental subduction: Geological Society of America Special Paper 403, p. 1–22.

Liati, A., and Gebauer, D., 1999, Constraining the prograde and retrograde P-T-t path of Eocene HP rocks by SHRIMP dating of different zircon domains: inferred rates of heating, burial, cooling and exhumation for central Rhodope, northern Greece: Contributions to Mineralogy and Petrology, v. 135, p. 340–354.

Liou, J. G., Zhang, R. Y., Katayama, I., and Maruyama, S., 2002, Global distribution and petrotectonic characterizations of UHPM terranes, *in* Parkinson, C. D., Katayama, I., Liou, J. G., and Maruyama, S., editors, The diamond-bearing Kokchetav massif, Kazakhstan: Tokyo, Japan, Universal Academy Press, p. 15–35.

Ludwig, K. R., 2001, Squid 1.02: A user's manual: Berkeley Geochronology Center Special Publication No. 2, 19 p.

——— 2003, User's manual for Isoplot 3.00: A geochronological toolkit for Microsoft Excel: Berkeley Geochronology Center Special Publication No. 4, 70 p.

Maas, R., Kinny, P. D., Williams, I. S., Froude, D. O., and Compston, W., 1992, The Earth's oldest known crust: A geochronological and geochemical study of 3900–4200 Ma detrital zircons from Mt. Narryer and Jack Hills, Western Australia: Geochimica et Cosmochimica Acta, v. 56, p. 1281–1300.
Massonne, H. J., and O'Brien, P. J., 2003, The Bohemian Massif and the NW Himalaya, *in* Carswell, D. A., and Compagnoni, R., editors, Ultrahigh Pressure Metamorphism, EMU Notes in Mineralogy, V. 5: Budapest, Eötvös University Press, p. 145–187.
Mattinson, C. G., Liou, J. G., Bird, D. K., Wooden, J. L., Wu, C., and Yang, J., 2005, Zircon geochronology and REE geochemistry, North Qaidam UHP terrane, northwest China: Mitteilungen der Österreichischen Mineralogischen Gesellschaft, v. 150, p. 106.
Mattinson, C. G., Wooden, J. L., Liou, J. G., Bird, D. K., and Wu, C. L., 2006, Geochronology and tectonic significance of Middle Proterozoic granitic orthogneiss, North Qaidam HP/UHP terrane, Western China: Mineralogy and Petrology, v. 88, p. 227–241, doi:10.1007/s007/s00710-006-0149-1.
McClelland, W. C., Power, S. E., Gilotti, J. A., Mazdab, F. K., and Wopenka, B., 2006, U-Pb SHRIMP geochronology and trace element geochemistry of coesite-bearing zircons, North-East Greenland Caledonides, *in* Hacker, B. R., McClelland, B., and Liou, J. G., editors, Ultrahigh-Pressure Metamorphism: Deep Continental Subduction: Geological Society of America Special Paper 403, p. 23–43.
McDonough, W. F., and Sun, S. S., 1995, The composition of the Earth: Chemical Geology, v. 120, p. 223–253.
Menold, C. A., Manning, C. E., Yin, A., and Chen, X., 2004, Geology of the North Qaidam HP-UHP terrane, Western China: American Geophysical Union, Eos Transactions, v. 85, p. F1679.
Menold, C. A., Yin, A., and Manning, C. E., 2005, Tectonic evolution of the North Qaidam UHP terrane: Mitteilungen der Österreichischen Geologischen Gesellschaft, v. 150, p. 109.
Newton, R. C., and Kennedy, G. C., 1963, Some equilibrium reactions in the join $CaAl_2Si_2O_8$–H_2O: Journal of Geophysical Research, v. 68, p. 2967–2983.
Okrusch, M., Seidel, E., and Davis, E., 1978, The assemblage jadeite–quartz in the glaucophane rocks of Sifnos (Cyclades Archipelago, Greece): Neues Jahrbuch für Mineralogie, Abhandlungen, v. 132, p. 284–308.
Pan, Y., 1997, Zircon- and monazite-forming metamorphic reactions at Manitouwadge, Ontario: Canadian Mineralogist, v. 35, p. 105–118.
Pearce, N. J. G., Perkins, W. T., Westgate, J. A., Gorton, M. P., Jackson, S. E., Neal, C. R., and Chenery, S. P., 1997, A compilation of new and published major and trace element data for NIST SRM 610 and NIST SRM 612 glass reference materials: Geostandards Newsletter, v. 21, p. 115–144.
Pidgeon, R. T., Furfaro, D., Kennedy, A. K., Nemchin, A. A., and van Bronswjk, W., 1994, Calibration of zircon standards for the Curtin SHRIMP II: U.S. Geological Survey Circular, v. 1107, p. 251.
Pognante, U., 1989, Lawsonite, blueschist and eclogite formation in the southern Sesia zone (western Alps, Italy): European Journal of Mineralogy, v. 1, p. 89–104.
Poli, S., and Schmidt, M. W., 1995, H_2O transport and release in subduction zones: Experimental constraints on basaltic and andesitic systems: Journal of Geophysical Research, v. 100, p. 22299–22314.
Rubatto, D., 2002, Zircon trace element geochemistry: partitioning with garnet and the link between U-Pb ages and metamorphism: Chemical Geology, v. 184, p. 123–138.
Rubatto, D., and Hermann, J., 2001, Exhumation as fast as subduction?: Geology, v. 29, p. 3–6.
——— 2003, Zircon formation during fluid circulation in eclogites (Monviso, Western Alps): Implications for Zr and Hf budget in subduction zones: Geochimica et Cosmochimica Acta, v. 67, p. 2173–2187.
Rubatto, D., and Scambelluri, M., 2003, U-Pb dating of magmatic zircon and metamorphic baddeleyite in the Ligurian eclogites (Voltri Massif, Western Alps): Contributions to Mineralogy and Petrology, v. 146, p. 341–355.
Rubatto, D., Gebauer, D., and Compagnoni, R., 1999, Dating of eclogite-facies zircons: the age of Alpine metamorphism in the Sesia-Lanzo Zone (Western Alps): Earth and Planetary Science Letters, v. 167, p. 141–158.
Rubin, J. N., Henry, C. D., and Price, J. G., 1993, The mobility of zirconium and other "immobile" elements during hydrothermal alteration: Chemical Geology, v. 110, p. 29–47.
Schulte, B., and Sindern, S., 2002, K-rich fluid metasomatism at high-pressure metamorphic conditions: Lawsonite decomposition in rodingitized ultramafite of the Maksyutovo Complex, Southern Urals (Russia): Journal of Metamorphic Geology, v. 20, p. 529–541.
Searle, M., Hacker, B. R., and Bilham, R., 2001, The Hindu Kush seismic zone as a paradigm for the creation of ultrahigh-pressure diamond-and coesite-bearing continental rocks: Journal of Geology, v. 109, p. 143–153.
Smith, D. C., 1984, Coesite in clinopyroxene in the Caledonides and its implications for geodynamics: Nature, v. 310, p. 641–644.
Sobolev, N. V., and Shatsky, V. S., 1990, Diamond inclusions in garnets from metamorphic rocks: a new environment for diamond formation: Nature, v. 343, p. 742–746.
Song, S., Yang, J., Katayama, I., Liu, F., and Maruyama, S., 2001a, Zircons and their inclusions from various rocks in the Dulan UHP metamorphic terrane, the North Qaidam, NW China, UHPM workshop 2001: Fluid/slab/mantle interactions and ultrahigh-P minerals: Tokyo, Japan, Waseda University, p. 116–120.
Song, S., Yang, J., Wu, C., Liou, J. G., and Xu, Z., 2001b, Petrology, geochemistry, and isotopic ages of eclogites in the Dulan UHPM terrane, the North Qaidam, NW China, Sixth International Eclogite Conference: Niihama, Japan, p. 150.
Song, S., Yang, J., Liou, J. G., Wu, C., Shi, R., and Xu, Z., 2003a, Petrology, geochemistry and isotopic ages of eclogites from the Dulan UHPM terrane, the North Qaidam, NW China: Lithos, v. 70, p. 195–211.
Song, S. G., Yang, J. S., Xu, Z. Q., Liou, J. G., and Shi, R. D., 2003b, Metamorphic evolution of the coesite-bearing ultrahigh-pressure terrane in the North Qaidam, Northern Tibet, NW China: Journal of Metamorphic Geology, v. 21, p. 631–644.

Song, S., Zhang, L., Niu, Y., Su, L., Jian, P., and Liu, D., 2005, Geochronology of diamond-bearing zircons from garnet peridotite in the North Qaidam UHPM belt, Northern Tibetan Plateau: A record of complex histories from oceanic lithosphere subduction to continental collision: Earth and Planetary Science Letters, v. 234, p. 99–118.

Song, S., Zhang, L., Niu, Y., Li, S., Song, B., and Liu, D., 2006, Evolution from oceanic subduction to continental collision: a case study from the northern Tibetan Plateau based on geochemical and geochronological data: Journal of Petrology, v. 47, p. 435–455.

Spandler, C., Hermann, J., Arculus, R., and John, M., 2003, Redistribution of trace elements during prograde metamorphism from lawsonite blueschist to eclogite facies; implications for deep subduction-zone processes: Contributions to Mineralogy and Petrology, v. 146, p. 205–222.

Stacey, J. S., and Kramers, J. D., 1975, Approximation of terrestrial lead isotope evolution by a two-stage model: Earth and Planetary Science Letters, v. 26, p. 207–221.

Steiger, R. H., and Jäger, E., 1977, Subcommission on geochronology: Convention on the use of decay constants in geo- and cosmochemistry: Earth and Planetary Science Letters, v. 36, p. 359–362.

Stöckhert, B., and Gerya, T. V., 2005, Pre-collisional high pressure metamorphism and nappe tectonics at active continental margins: a numerical simulation: Terra Nova, v. 17, p. 102–110.

Tera, F., and Wasserburg, G. J., 1972, U-Th-Pb systematics in three Apollo 14 basalts and the problem of initial Pb in lunar rocks: Earth and Planetary Science Letters, v. 14, p. 281–304.

Terry, M. P., Robinson, P., Hamilton, M. A., and Jercinovic, M. J., 2000, Monazite geochronology of UHP and HP metamorphism, deformation, and exhumation, Nordøyane, Western Gneiss Region, Norway: American Mineralogist, v. 85, p. 1651–1664.

Tribuzio, R., Messiga, B., Vannucci, R., and Bottazzi, P., 1996, Rare earth element redistribution during high-pressure–low-temperature metamorphism in ophiolitic Fe-gabbros (Liguria, northwestern Italy): Implications for light REE mobility in subduction zones: Geology, v. 24, p. 711-714.

Usui, T., Nakamura, E., Kobayashi, K., Maruyama, S., and Helmstaedt, H., 2003, Fate of the subducted Farallon plate inferred from eclogite xenoliths in the Colorado Plateau: Geology, v. 31, p. 589-592.

Usui, T., Nakamura, E., and Helmstaedt, H., 2006, Petrology and geochemistry of eclogite xenoliths from the Colorado Plateau: Implications for the evolution of subducted oceanic crust: Journal of Petrology, v. 47, p. 929–964.

Wan, Y., Zhang, J., Yang, J., and Xu, Z., 2006, Geochemistry of high-grade metamorphic rocks of the North Qaidam mountains and their geological significance: Journal of Asian Earth Sciences, doi:10.1016/j.jseaes.2005.09.018.

Whitehouse, M. J., and Platt, J. P., 2003, Dating high-grade metamorphism–constraints from rare-earth elements in zircon and garnet: Contributions to Mineralogy and Petrology, v. 145, p. 61–74.

Williams, I. S., 1998, U-Th-Pb geochronology by ion microprobe, *in* McKibben, M. A., Shanks, W. C., III, and Ridley, W. I., editors, Applications of microanalytical techniques to understanding mineralizing processes: Society of Economic Geologists, Reviews in Economic Geology, v. 7, p. 1–35.

Wu, C., Yang, J., Wooden, J., Ernst, W. G., Liou, J. G., Li, H., Zhang, J., Wan, Y., and Shi, R., 2001, Relationship between UHP eclogite and two different types of granite in the North Qaidam, NW China: Evidence from zircon SHRIMP ages of granites: American Geophysical Union, Eos Transactions, v. 82, p. Abstract V32C-0980.

Wu, C., Yang, J., Wooden, J. L., Shi, R., Chen, S., Meibom, A., and Mattinson, C., 2004, Zircon U-Pb SHRIMP dating of the Yematan Batholith in Dulan, north Qaidam, NW China: Chinese Science Bulletin, v. 49, p. 1736–1740.

Yang, J., Wu, C., Zhang, J., Song, S., and Ireland, T. R., 2001a, U-Pb/Sm-Nd/Ar-Ar ages of the North Qaidam ultrahigh-high pressure metamorphic rocks, NW China, Sixth International Eclogite Conference: Niihama, Japan, p. 178.

Yang, J., Xu, Z., Zhang, J., Chu, C. Y., Zhang, R., and Liou, J. G., 2001b, Tectonic significance of Early Paleozoic high-pressure rocks in Altun–Qaidam–Qilian Mountains, NW China: Geological Society of America Memoir, v. 194, p. 151–170.

Yang, J., Song, S., Xu, Z., Wu, C., Mattinson, C., Bian, A., Zhang, R. Y., Liou, J. G., and Ernst, W. G., 2001c, Northern Qaidam Caledonian UHP terrane: A new discovery: American Geophysical Union, Eos Transactions, v. 82, p. F1342.

Yang, J., Xu, Z., Zhang, J., Song, S., Wu, C., Shi, R., Li, H., and Brunel, M., 2002, Early Paleozoic North Qaidam UHP metamorphic belt on the northeastern Tibetan plateau and a paired subduction model: Terra Nova, v. 14, p. 397–404.

Yang, J. J., Zhu, H., Deng, J. F., Zhou, T. Z., and Lai, S. C., 1994, Discovery of garnet-peridotite at the northern margin of the Qaidam basin and its significance: Acta Petrologica et Mineralogica, v. 13, p. 97–105 (in Chinese with English abstract).

Yang, J. S., Xu, Z. Q., Li, H. B., Wu, C. L., Cui, J. W., Zhang, J. X., and Chen, W., 1998, Discovery of eclogite at northern margin of Qaidam basin, NW China: Chinese Science Bulletin, v. 43, p. 1755–1760 (in Chinese with English abstract).

Yin, A., and Harrison, T. M., 2000, Geologic evolution of the Himalayan-Tibetan orogen: Annual Review of Earth and Planetary Sciences, v. 28, p. 211–280.

Zack, T., Rivers, T., Brumm, R., and Kronz, A., 2004, Cold subduction of oceanic crust: Implications from a lawsonite eclogite from the Dominican Republic: European Journal of Mineralogy, v. 16, p. 909–916.

Zhang, J. X., Mattinson, C. G., Meng, F. C., and Wan, Y. S., 2005a, An Early Palaeozoic HP/HT granulite-garnet peridotite association in the south Altyn Tagh, NW China: P-T history and U-Pb geochronology: Journal of Metamorphic Geology, v. 23, p. 491–510.

Zhang, J. X., Yang, J. S., Mattinson, C. G., Xu, Z. Q., Meng, F. C., and Shi, R. D., 2005b, Two contrasting eclogite cooling histories, North Qaidam HP/UHP terrane, western China: Petrological and isotopic constraints: Lithos, v. 84, p. 51–76.